MOLECULAR DYNAMICS STUDY OF Aβ MONOMERS AND OLIGOMERS INTERACTING WITH COFACTORS

by

Seongwon Kim

A Dissertation
Submitted to the
Graduate Faculty
of
George Mason University
in Partial Fulfillment of
The Requirements for the Degree
of
Doctor of Philosophy
Bioinformatics and Computational Biology

Committee:

_____ Dr. Dmitri Klimov, Dissertation Director

_____ Dr. Saleet Jafri, Committee Member

_____ Dr. Iosif Vaisman, Committee Member

_____ Dr. Igor Griva, Committee Member

_____ Dr. James Willet, Director, School of Systems Biology

_____ Dr. Timothy L. Born, Associate Dean for Student and Academic Affairs, College of Science

_____ Dr. Vikas Chandhoke, Dean, College of Science

Date: _____ Spring Semester 2013
George Mason University
Fairfax, VA

Molecular Dynamics Study of Aβ Monomers and Oligomers Interacting with Cofactors

A dissertation submitted in partial fulfillment of the requirements for the degree of Doctor of Philosophy at George Mason University

By

Seongwon Kim
Doctor of Philosophy
New York University, 1998

Director: Dmitri Klimov, Associate Professor
School of Systems Biology

Spring Semester 2013
George Mason University
Manassas, VA

ACKNOWLEDGEMENTS

First of all, I would like to thank Dr. Klimov, my dissertation director. He guided the thorough course of my study and shared invaluable time, idea and insights in research and publication. Working with him will remain to be the crucial factor in the formative stage of my scientific career. I also thank my dissertation committee, Dr. Griva, Dr. Jafri, and Dr. Vaisman for their time and advice during my research.

Great thanks go to my family. My precious treasures Charles, Chris and Katie have comforted and consoled me during challenging times. A very special place is reserved for my beloved wife, Eunice, who deserves more thanks than anyone for her patience, devotion and encouragement.

I wish to acknowledge the presidential scholarship and teaching assistantship from George Mason University during my graduate study.

TABLE OF CONTENTS

PAGE

LIST OF TABLES……vi

LIST OF FIGURES……vii

ABSTRACT……viii

1. INTRODUCTION……...1

2. RESEARCH AIMS……5

3. METHODS……..6

3.1 CHARMM19+SASA model 6

3.1.1 Building naproxen parametrization 7

3.1.2 Building DMPC lipid parametrization 7

3.2 Simulation systems 9

3.2.1 Aβ monomer and oligomers in water 9

3.2.2 Aβ dimer coincubated with naproxen 9

3.2.3 Building the DMPC monolayer model 10

3.3 Replica Exchange Molecular Dynamics (REMD) 14

3.4. Structural probes 15

3.4.1 Structural probes for Aβ peptides 15

3.4.2 Structural probes for naproxen 16

3.4.3 Structural probes for DMPC monolayer 17

4. STRUCTURES AND CONFORMATIONS OF Aβ OLIGOMERS……....18

4.1 Results 18

4.1.1 Thermodynamics of Aβ oligomer assembly 18

4.1.2 Structure of Aβ oligomers 23

4.1.3 Conformational propensities of Aβ oligomers and monomers 25

4.1.4 Conformational clusters of Aβ oligomers and monomers 28

4.2 Discussion 32

4.2.1 Aβ oligomerization is a continuous process 32

4.2.2 Structural properties of Aβ dimers and tetramers are similar 33

4.2.3 Conformations of Aβ peptides in dimers and tetramers are similar 33
4.2.4 Conformations of Aβ peptides in oligomers and monomers are distinct..... 34
4.2.5 Comparison with experiments 35
4.3 Conclusion 36
5. Aβ DIMER COINCUBATED WITH NAPROXEN……37
5.1 Results..... 37
5.1.1 Naproxen destabilizes Aβ dimer..... 37
5.1.2 Naproxen binding to Aβ dimer affects interpeptide interaction 43
5.1.3 Naproxen binding to Aβ dimer is governed by Aβ sequence 45
5.2 Discussion..... 47
5.2.1 Mechanism of naproxen antiaggregation effect..... 47
5.2.2 Naproxen binds to Aβ dimers and fibrils via different mechanisms 48
5.2.3 Comparison with experiments 50
5.3 Conclusion 51
6. INTERACTION OF Aβ MONOMER WITH LIPID MONOLAYER……52
6.1 Results..... 52
6.1.1 Binding of Aβ to lipid monolayer..... 52
6.1.2 Impact of monolayer binding on the structure of Aβ..... 54
6.1.3 Clustering of the structural ensemble of Aβ monomer..... 58
6.1.4 Impact of Aβ binding on the lipid monolayer..... 61
6.2 Discussion..... 63
6.3 Conclusion 67
7. CONCLUSIONS AND FUTURE WORK……68
APPENDIX……70
REFERENCES ……..75
CURRICULUM VITAE……...…….……..82

LIST OF TABLES

Table Page
1. Table 1 29
2. Table 2 30
3. Table 3 30

LIST OF FIGURES

Figure Page
1. Figure 1 9
2. Figure 2 11
3. Figure 3 12
4. Figure 4 13
5. Figure 5 17
6. Figure 6 19
7. Figure 7 21
8. Figure 8 22
9. Figure 9 24
10. Figure 10 26
11. Figure 11 27
12. Figure 12 31
13. Figure 13 37
14. Figure 14 40
15. Figure 15 42
16. Figure 16 44
17. Figure 17 45
18. Figure 18 53
19. Figure 19 54
20. Figure 20 55
21. Figure 21 57
22. Figure 22 59
23. Figure 23 62
24. Figure 24 65

ABSTRACT

MOLECULAR DYNAMICS STUDY OF Aβ MONOMERS AND OLIGOMERS INTERACTING WITH COFACTORS

Seongwon Kim, Ph.D.

New York University, 1998

Thesis Director: Dr. Dmitri Klimov

Amyloid-β peptides are implicated in the Alzheimer's disease (AD), an age-related neurodegenerative disorder. In this work, we study the dynamics of Aβ monomer and oligomers in water and interacting with cofactors such as naproxen or lipid monolayer. All-atom force field combined with fast implicit solvent model and replica exchange molecular dynamics is used to obtain exhaustive sampling of Aβ monomer and oligomer conformations in water. Similar methodology is used to study the interaction of Aβ dimer and naproxen. The antiaggregation effect and the utility of naproxen as pharmaceutical agent against AD are discussed. In an attempt to understand the Aβ-membrane interaction which is believed to be responsible for cell toxicity, we study the interaction of Aβ monomer and lipid monolayer. A new force field for DMPC monolayer consistent with CHARMM19+SASA model is presented. A reliable statistical analysis of Aβ monomer bound to DMPC monolayer demonstrates that membrane interaction profoundly perturbs the structures of both the peptide and lipid monolayer.

1. INTRODUCTION

Alzheimer's Disease (AD) is the most common form of aged-related, progressive neurodegenerative disorder. It leads to memory loss, cognitive disability and deteriorated mobility, causing the patient's complete loss of independence and eventual death. The number of AD patients worldwide was estimated to be 26.6 million as of 2006, which is anticipated to quadruple by 2050 [1]. The devastating effect of AD is particularly pronounced in modern society with longer life expectancy. The demand for patient care and economic burden that ensues make the AD one of the severest challenges today.

Examination of post mortem brains of AD patients uncovered extracellular senile plaque formed by amyloid fibrils [2]. The fibrils were initially misunderstood to be starch-like deposits, consisting of carbohydrates or "amyloids". Further research revealed that they are composed of Aβ peptides, produced by the action of β and γ secretases on the amyloid precursor protein (APP) [3]. Mutations around the enzymatic cleavage sites of APP were discovered to be linked to the disease, leading to the formulation of the amyloid cascade hypothesis, namely, the aggregation of Aβ peptides may be the cause of AD [2].

Among naturally occurring Aβ peptides, $A\beta_{1-40}$ is most abundant in human body, while $A\beta_{1-42}$ is more prone to aggregation and more toxic [4]. Even though $A\beta_{1-40}$ and $A\beta_{1-42}$ differ only by two terminal amino acids (Ile and Ala), their monomers and oligomers

exhibit different distributions with respect to oligomer order (i.e. the number of peptides in the aggregate) in aqueous environment [4] and distinct structures [5, 6]. Computational studies of Aβ peptides showed that $A\beta_{1-40}$ and $A\beta_{1-42}$ aggregation follows distinct pathways [7, 8]. Aβ monomers lack stable secondary or tertiary structure in aqueous environment, forming a complex ensemble of interchanging structures [5, 9]. They undergo aggregation processes involving polymorphic structural transitions between oligomeric species, eventually forming the amyloid fibrils with characteristic cross-β structures [10, 11, 12].

More recently, experimental evidences have established that the main causative agent in the pathogenesis of AD is the soluble Aβ oligomers rather than amyloid fibrils [13, 14]. Indeed, neurotoxicity is found to better correlate with the concentration of Aβ oligomers rather than fibrils [15]. Furthermore, structural stabilization of Aβ peptides via fibrillation was shown to diminish their cytotoxic effect [16]. On the other hand, oligomers as small as dimers are shown to exhibit neurotoxicity [17]. Experimental [18] and computational [19] studies have indicated that monomer to oligomer transition enhances the strand content of Aβ peptides, which may serve as an indicator of their cytotoxicity [18].

Active research has been focused on finding or designing small molecule therapeutic agents that can inhibit or diminish cytotoxic effect of Aβ peptides. Specifically, it has been discovered that long-term treatment with non-steroidal anti-inflammatory drugs (NSAIDs) can significantly reduce the risk or delay the onset of AD [20]. Experiments on

antiaggregation effect of NSAIDs against Aβ fibrils have been reported [21]. Among the NSAIDs tested, ibuprofen and naproxen provided the strongest anti-aggregation effect [22]. In particular, when the patients with preexisting conditions are excluded, naproxen reduces the risk of AD by 67% [20]. However, in mice models naproxen cannot reverse existing AD conditions in brain microglia [23]. Recently, computational studies have been performed to investigate the antiaggregation effect of NSAIDs against Aβ fibrils [24, 25, 26]. Since the major cytotoxic species are Aβ oligomers, it is interesting to study their interaction of NSAIDs such as naproxen.

There has been considerable research on the cause of cytotoxicity of Aβ oligomers. Of special significance is the effect of interaction between Aβ oligomers and cellular membranes [27, 28]. Studies have indicated that Aβ peptide has strong propensity to interact with membrane environment. Numerous experimental and computational studies have shown that natural or artificial interface environment may have catalytic effect for enhancing β-structure [29, 30], which may also contribute to the fibrillation process. Such interface surfaces include membrane-mimicking detergents [31], octane and water [32] and air-water interface [33]. Shea and coworkers [34] have studied the effect of β-propensity on the aggregation of coarse-grained model of peptides on hydrophobic surfaces. On the other hand, Aβ peptides are shown to perturb membrane structures [35, 36] and properties, such as conductivity, permeability and fluidity [37, 38]. Especially, it is believed that Aβ oligomers can form cellular pores or channel structures that can deteriorate cellular homeostasis of cations such as Ca^{2+} [39, 40, 41]. Simplified models of

peptide and lipid have demonstrated how the peptide oligomerization on the micelle surface can lead to the leakage of inner-micelle components [42]. This loss of ionic homeostasis may play crucial role in the neuronal cell death, leading to the AD.

Experimental elucidation of the precise structural properties of Aβ peptides interacting with ligands or membranes is a very difficult task due to their transient nature. Recently, computational methodology such as Molecular Dynamics (MD) has achieved remarkable progress for tackling such problems, enabling one to access atomistic details of many systems of biological relevance. In this study, we use MD to investigate the Aβ peptides in water or interacting with naproxen or lipid membrane. To meet the computational challenge, we employ the SASA (Solvent Accessible Surface Area) model [43] combined with the CHARMM19 force field. Comparison of aqueous environment and naproxen solution will help us delineate the nature of naproxen-Aβ interaction and assess therapeutic utility of naproxen against AD. We have also obtained exhaustive MD sampling of $A\beta_{10\text{-}40}$ monomer interacting with lipid monolayer using SASA solvent model. These simulations are expected to be useful in understanding the interactions of Aβ peptides with cellular membranes and, potentially, the mechanism of Aβ cytotoxicity. The results presented in this dissertation are published in [44, 45, 46, 47].

2. RESEARCH AIMS

The aim of this dissertation can be stated as follows.

1. Use REMD to study the structure and conformational ensemble of Aβ monomers and oligomers up to tetramer. Analyze geometrical properties and their thermodynamic behavior, with particular emphasis on the comparison of dimer and tetramer. Characterize the thermodynamics of oligomerization by analyzing the free energy of aggregation and its interface. Study the impact of peptide interaction on the secondary structure and the structural changes compared to monomer. Employ clustering methodology to analyze conformational ensembles of Aβ oligomers and monomer.
2. Use REMD to explore the impact of naproxen on Aβ oligomerization. Quantify the nature of destabilizing effect of naproxen. Analyze structural characteristics of Aβ dimer coincubated with naproxen and compare them with those in aqueous environment. Study the free energy of oligomerization in the vicinity of naproxen and compare it with the cases of dimerization in water or fibrillation. Infer the utility of naproxen as a therapeutic agent against Alzheimer's disease.
3. Devise a novel force field for DMPC lipid suitable for CHARMM19+SASA implicit solvent model. Design a lipid monolayer model and study its interaction with Aβ monomer. Investigate the impact of binding on the structures of both peptide and lipids.
4. Compare the simulation results with experiments.

3. METHODS

In this work, we study the N-terminal truncated $A\beta_{10\text{-}40}$ peptide as a model of full length $A\beta_{1\text{-}40}$. This choice is motivated by a recent computational study, which has demonstrated that amino-terminal truncated $A\beta_{10\text{-}40}$ can be used as a good model for full length $A\beta_{1\text{-}40}$ in oligomer conformations [48]. The primary sequence of $A\beta_{10\text{-}40}$ is as follows: $Y_{10}EVHHQKLVFF_{20}AEDVGSNKGA_{30}IIGLMVGGVV_{40}$.

3.1 CHARMM19+SASA model

To study the combined system of Aβ peptide(s) and cofactors, we use CHARMM program [49] and united atom force field CHARMM19 equipped with SASA model for implicit solvent [43]. SASA uses analytical approximations to estimate the solvation energy of atoms in molecules based on interatomic distances. It employs solvation coefficient for each atom type, where N and O atoms reduce, while C and S atoms increase the solvation energy. SASA also uses knowledge-based probabilistic coefficients for different atom types, which were obtained using small peptides in water. Our choice of this model was motivated by the previous studies of Aβ peptides in aqueous environment. For example, CHARMM19+SASA model successfully reproduced the chemical shifts of Cα and Cβ atoms in Aβ monomer [13] and β-strand content of Aβ monomer and oligomers up to tetramer [9]. It also reproduced the dock and lock

mechanisms of Aβ fibrillation, the onset of which were shown to occur at the temperatures consistent with experiments [50].

3.1.1 Building naproxen parametrization

The parametrization of naproxen consistent with CHARMM19+SASA model was performed in [25], using the similarity of its structural groups with amino acids. We employ this parametrization in this work as well.

3.1.2 Building DMPC lipid parametrization

A major contribution of the present study is building a force field parametrization for DMPC lipid. Standard force fields for lipids include CHARMM27, Berger's and Amber. However, these force fields employ explicit solvent models which are computationally expensive. Specifically, to utilize computational efficiency of implicit solvent model we need to develop a CAHRMM19+SASA parametrization for DMPC. To this end, we can exploit the similarity of the lipid groups with aliphatic amino acids and nucleic acids. Similar attempt has been also made by Pande [51], based on CHARMM19 force field combined with nucleic acid parameters of Karplus [52].

Standard nitrogen, carbon and oxygen atom types from CHARMM19 force field were used for DMPC model. Similar to CHARMM27 force field, atom type OS is used for both oxygen atoms forming double bonds in ester groups and phosphorus group. Since

the remaining atom types in the phosphorus group require novel nomenclature, we utilized the atom types OT and LP from SASA, which have no counterparts in CHARMM19 force field for amino acids. We assume that the atom types OS and OT have the same probabilistic and solvation energetic coefficients in SASA model as the other oxygen atom types. Solvation effect of phosphorus atom type LP was neglected, as in [53]. Partial charges were taken from CHARMM27 force field, by assigning appropriate sums of individual partial charges to united hydrocarbon atoms. Lennard-Jones parameters for atom types OT and LP were taken from united atom force field for nucleic acids [52]. The bond length, bond angle and dihedral angle parameters were taken from the CHARMM19 force field. For those interactions involving OS, OT and LP, we used the parameters obtained from explicit water CHARMM19 parametrization [51]. Missing parameters were assigned to provide an agreement with the experimental data.

To validate our parametrization, we ran a test simulation of a single DMPC lipid molecule both in our CHARMM19+SASA model and in explicit water CHARMM27 force field. We found that dihedral angle distributions in both simulations generally showed good agreements, except for the angles θ_1, β_2 and γ_2 (**Figure 1**). To enforce their consistency, we added extra terms for those angles in the topology and parameter files. The resulting implicit solvent model of DMPC lipids is described in the Appendix.

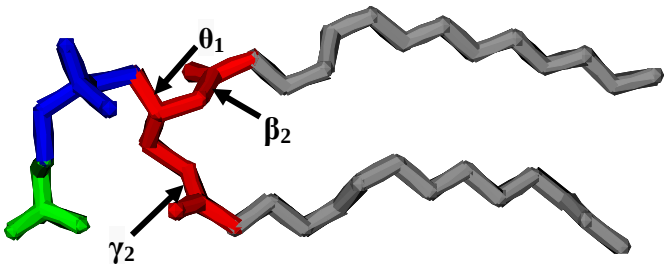

Figure 1 *The structure of a DMPC molecule in united-atom scheme. Functional groups of the lipid are shown in green (choline), blue (phosphorus), red (glycerol) and gray (fatty acid). Dihedral angles θ_1, β_2 and γ_2 are shown.*

3.2 Simulation systems

3.2.1 Aβ monomer and oligomers in water

Aβ monomer, dimer or tetramer were placed in a sphere with the radius R_s = 90 Å. The spherical boundary condition was represented by a soft harmonic potential with the force constant k_s = 10 kcal mol^{-1} Å $^{-2}$. Hence, the peptide concentration is on the order of mM. Initially, the peptides were unstructured and dissociated.

3.2.2 Aβ dimer coincubated with naproxen

Aβ dimer was prepared as above. Then 20 naproxen molecules were randomly placed in the vicinity of the dimer. Hence, the ligand to peptide ratio is 10:1, which is within experimental range.

3.2.3 Building the DMPC monolayer model

We built the DMPC monolayer system using 81 lipids (**Figure 2**). The system size was 70.2 Å x 70.2 Å x 102 Å. We employed periodic boundary condition and particle mesh Ewald method for computing electrostatic interactions. Preliminary simulations have shown that the SASA model produces excessive hydrophobic interaction in the lipid tail region, resulting in partial collapse of the lipid system. Since our attempts to tune the SASA coefficients to reproduce correct lipid membrane structure were unsatisfactory, we softly constrained the P atoms in lipid headgroups to z = 0 Å plane with the force constant k = 0.6 kcal mol^{-1} Å^{-2}. To mimic the presence of lower leaflet of the lipid bilayer, we placed a planar layer of hydrophobic atoms below the lipid tails. We used 324 atoms in the layer, making the ratio of lipid to hydrophobic layer atoms to be 1:4. The hydrophobic layer was constrained at z = -22 Å using the constant k = 5 kcal mol^{-1} Å^{-2}. The specific position of the layer was determined so that the order parameter S_{cd} for the lipid tail will best reproduce experimental results [54], as shown in **Figure 3a**.

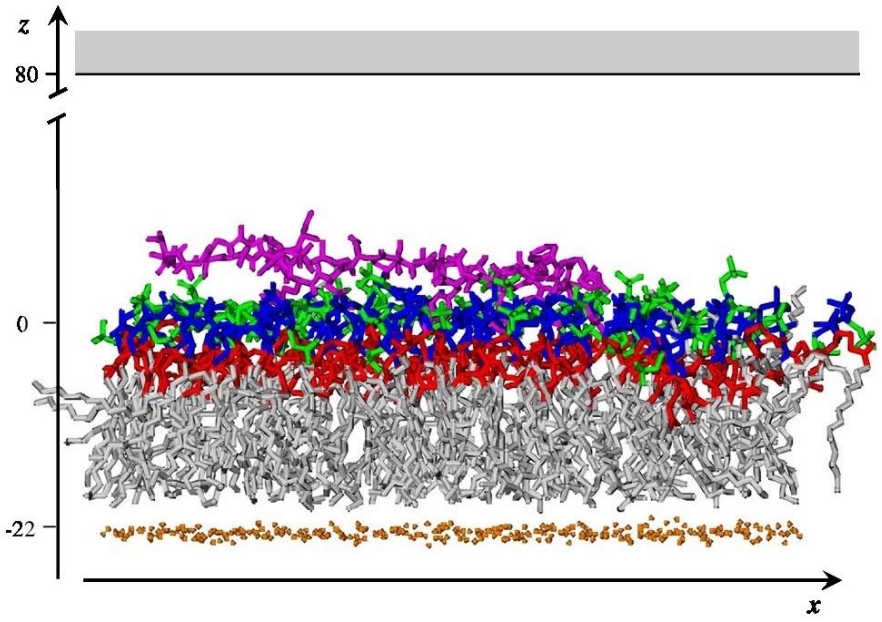

Figure 2 *Aβ and DMPC monolayer system. z-axis is normal to the monolayer. The phosphorus group is placed on z = 0 Å plane. For colors representing the lipids, see the caption of Figure 1. Peptide is represented in purple. The hydrophobic layer is shown in orange.*

In order to validate the monolayer model, we compared the distributions of the centers of mass of each lipid structural group (choline, phosphorus, glycerol and lipid tail) with the corresponding results from explicit solvent simulation using CHARMM27 force field (**Figure 3b**). The distributions agree well, with the SASA model showing somewhat smaller variations compared to the explicit solvent model.

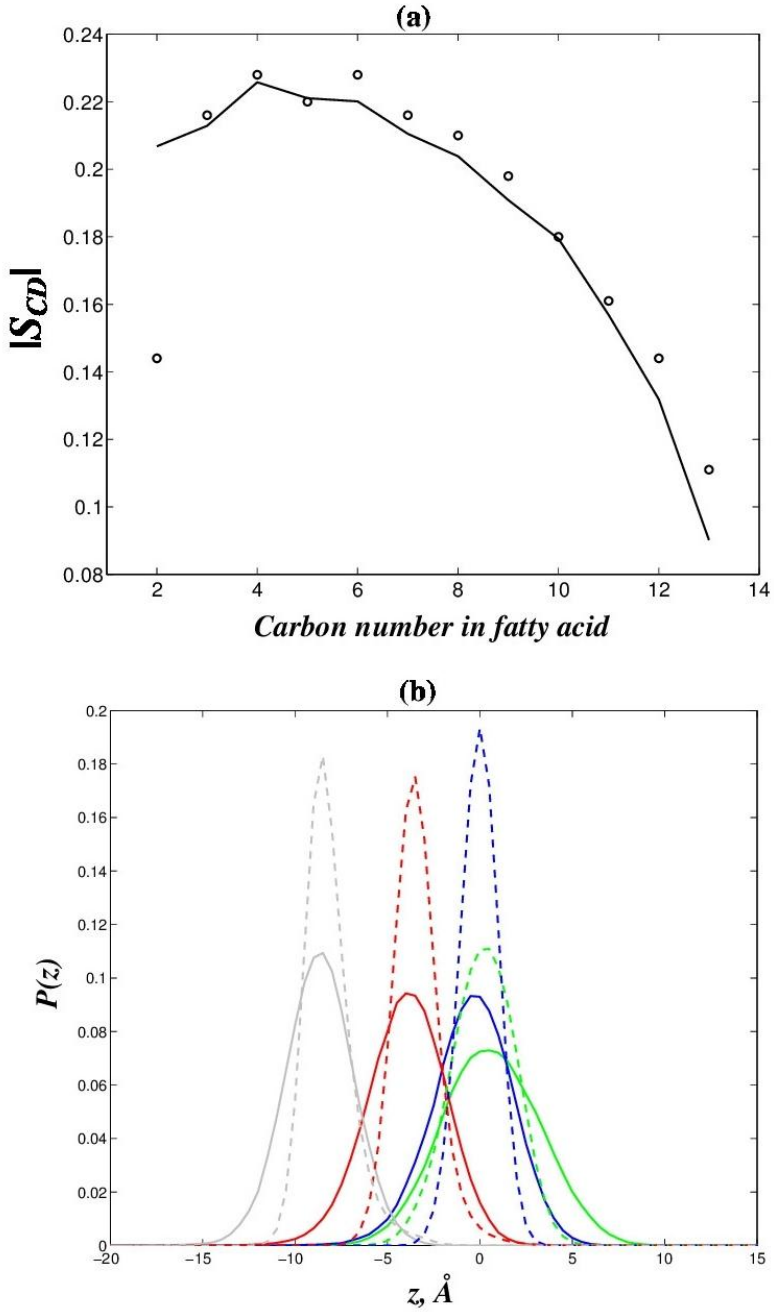

Figure 3 *(a) The lipid order parameter S_{cd} from experiment (circles) and our simulation (lines). (b) Distribution of z-coordinates of the centers of mass of choline (green), phosphorus (blue), glycerol (red) and fatty acid (gray) groups from explicit solvent (lines) and implicit solvent (dashed lines) simulations.*

In order to further validate our monolayer model in terms of its ability to reproduce membrane-amino acid interactions, we consulted the results from Tieleman [55] on the free energy profile of amino acid interacting wih DOPC bilayer. Their model used NPT ensemble at 298 K and OPLS-AA force field combined with SPC explicit water model. Specifically, we compared the results for Lys and Phe, as these residues turn out to be important for the Aβ-monolayer interaction. **Figure 4** shows that the free energy minimum for Lys lies near lipid head group (z ~ 0Å) due to favorable interaction between head group charges and Lys. We also note that Phe generally prefers to interact with hydrophobic core region of lipid monolayer, except for sharp rise of free energy near the artificial hydrophobic layer. Besides this artifact of our model, we observed that our monolayer simulations reproduce the behavior of Lys and Phe in lipid bilayer as in [55].

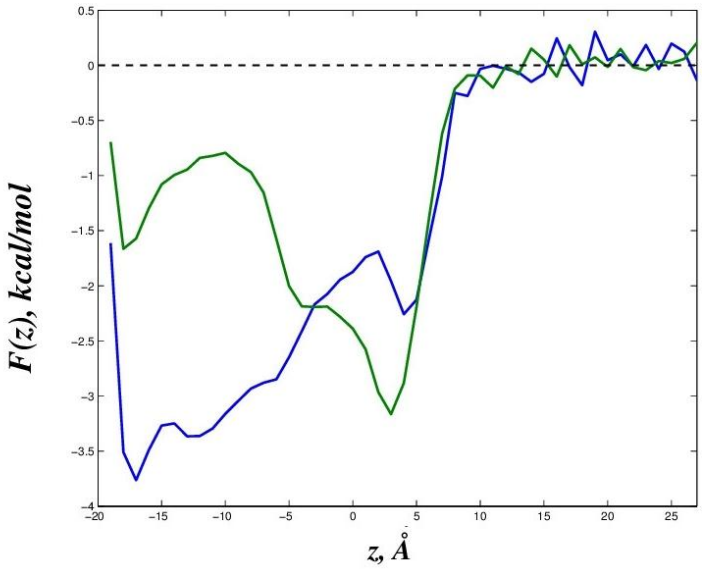

Figure 4 *Free energy along z-coordinate of Lys (green) and Phe (blue) relative to bulk water (F=0) obtained for our implicit solvent model of DMPC monolayer.*

3.3 Replica Exchange Molecular Dynamics (REMD)

To achieve the exhaustive sampling of our system, we utilized the REMD algorithm [56]. In this algorithm, replicas of the system are simulated in parallel at a wide range of temperatures. Periodically, the structures from replicas at neighboring temperatures are swapped with the probabilities derived from Metropolis-type criterion, thus preserving the equilibrium canonical distributions at each temperature. Velocity is rescaled in case of structure swapping to maintain the temperature at each replica. REMD method helps the structures to escape local minima at lower temperature and relax to the local minima at higher temperature.

For Aβ monomer and oligomers in water, we used 24 replicas whose temperatures were linearly distributed over 300 to 530 K. Exchange attempts were made every 80 ps, with the acceptance ratio of 67% (monomer), 54% (dimer) and 38% (tetramer). Between exchanges the system evolved using NVT underdamped Langevin dynamics with the damping coefficient γ = 0.15 ps^{-1} and the integration step of 2 fs. In all, 4 (monomer), 7 (dimer) and 8 (tetramer) trajectories were produced. After removing the initial equilibration steps, the analysis was done on the last 72 μs (monomer), 113 μs (dimer) and 126 μs (tetramer) of simulations.

For the Aβ dimer and naproxen system, the REMD protocol was the same as above; the acceptance ratio was 41%. In all, 13 trajectories were obtained, from which the last 227 μs was used for analysis.

To study our Aβ monomer bound to DMPC monolayer, we built 32 replicas whose temperatures were exponentially distributed from 330 to 560 K. The damping coefficient and integration steps were the same as for Aβ monomer system. Exchanges were attempted every 20 ps, with the acceptance ratio of about 26%. We obtained 5 trajectories, from which the last 30.7 μs were used for the analysis.

3.4. Structural probes

3.4.1 Structural probes for Aβ peptides

N-terminal and C-terminal of the Aβ are defined to be the sequence regions Tyr10-Asp23 and Gly29-Val39, respectively. Intrapeptide side chain contact is formed, if the distance between the centers of mass of two side chains is less than 6.5 Å. This approximately corresponds to the distance, at which the onset of hydration occurs. Hydrogen bond is defined according to Kabsch and Sander [57]. Secondary structures are defined according to the distribution of backbone dihedral angles (φ, ψ) as in [10]. Notice that it is different from that in the context of protein structures using hydrogen bonds.

In order to analyze the conformational ensemble of Aβ monomer, we employed the clustering method described in [58]. Each conformation is represented by a vector of 465 components, each taking the values of 1 or 0 according to the presence or absence of respective intrapeptide contact. Distance between two conformations is defined to be

Euclidean distance between the two vectors. The distance between a cluster and a conformation is defined to be the Euclidean distance between the centroid of the cluster and the vector. Cluster algorithm performs initial assignment of structures to clusters, taking into account the distances between structures. Then, the algorithm checks and if necessary reassigns the structures to the clusters. Iterations stop when the algorithm produces no more changes in cluster assignment.

The results of REMD simulation were analyzed using weighted histogram analysis method (WHAM) [59]. Throughout this work, <…> denotes the thermodynamic average. In order to facilitate the comparison of the present work with the results on Aβ oligomers in water or in fibril formation, we present the results and analysis at 360 K, which is the locking temperature for an incoming Aβ peptide interacting with preformed fibril [60].

3.4.2 Structural probes for naproxen

To analyze the simulation data, we represent naproxen molecule using three structural groups G1, G2 and G3, where G1 is hydrophobic naphthalene ring, G2 is the methoxy and G3 is the carboxylate group (**Figure 5).**

Contact between Aβ peptide and naproxen is assumed to be formed if the distance between the centers of mass of an amino acid and a structural group of naproxen is less than 6.5 Å. Ligand-ligand interaction is present, if the centers of mass of any structural groups in different naproxen molecules are less than 6.5 Å apart.

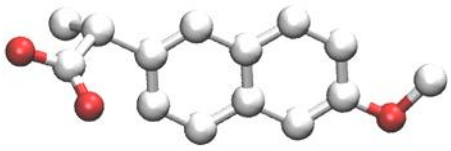

G3 **G1** **G2**

Figure 5 *Structure of naproxen molecule, with hydrophobic naphthalene ring (group G1), methoxy (G2), and carboxylate(G3) groups.*

3.4.3 Structural probes for DMPC monolayer

Aβ monomer and DMPC monolayer structures were analyzed using the following probes. To probe Aβ-lipid contacts, the DMPC lipid is divided into four structural groups: choline, phosphorus, glycerol and fatty acid (see **Figure 1** and Appendix). If the distance between the centers of mass of an amino acid side chain and a lipid structural group is less than 6.5 Å, a contact between that amino acid and lipid is assumed to be formed. Aβ is bound to the monolayer, if there is at least one contact between any amino acid and any lipid. The total number of contacts between Aβ and monolayer is defined to be the sum of all such contacts. In order to study the ordering of lipid tails represented in CHARMM19+SASA force field, we computed the order parameter S_{cd} employing the equation appearing in Essex et al. [61]. Specifically, for three consecutive Cα atoms C_{i-1}, C_i and C_{i+1} along the fatty acid chain, let **t** be the vector connecting C_{i-1} and C_{i+1}. Let **n** be the vector normal to C_{i-1}, C_i and C_{i+1} plane, and **b** be the vector normal to **t** and **n**. Define S_{nn} by $S_{nn} = ((3(\mathbf{n}\cdot\mathbf{z}) / |\mathbf{n}|)^2 - 1) / 2$. S_{bb} is defined similarly. Then the order parameter is given by $S_{cd} = (2 S_{nn} + S_{bb}) / 3$.

4. STRUCTURES AND CONFORMATIONS OF Aβ OLIGOMERS

4.1 Results

4.1.1 Thermodynamics of Aβ oligomer assembly

In **Figure 6a** we present the free energy profile of Aβ oligomers with respect to the number of interpeptide hydrophobic contacts C_h at 360 K, where the probability to form tetramer is ~ 1.0. For both dimer and tetramer, the free energy profile has a single minimum near C_h = 5 (dimer) or C_h = 10 (tetramer). This suggests that the oligomerization is a barrierless, continuous process. The free energy minima for dimer and tetramer are -3.7RT and -6.4RT, respectively, so the tetramer formation is more stable compared to dimer by the difference in free energy of 2.7RT. **Figure 6b** shows that the system free energy as a function of T has a single maximum at $T = T_o$, where T_o = 382 K for tetramer and 371 K for dimer. We interpret T_o as the temperature of oligomerization. Importantly, the system free energy can be matched with quadratic function $F(T) \sim -(T - T_o)^2$ for $T < T_o$, which is also consistent with the observation that oligomerization is a continuous phase transition [62].

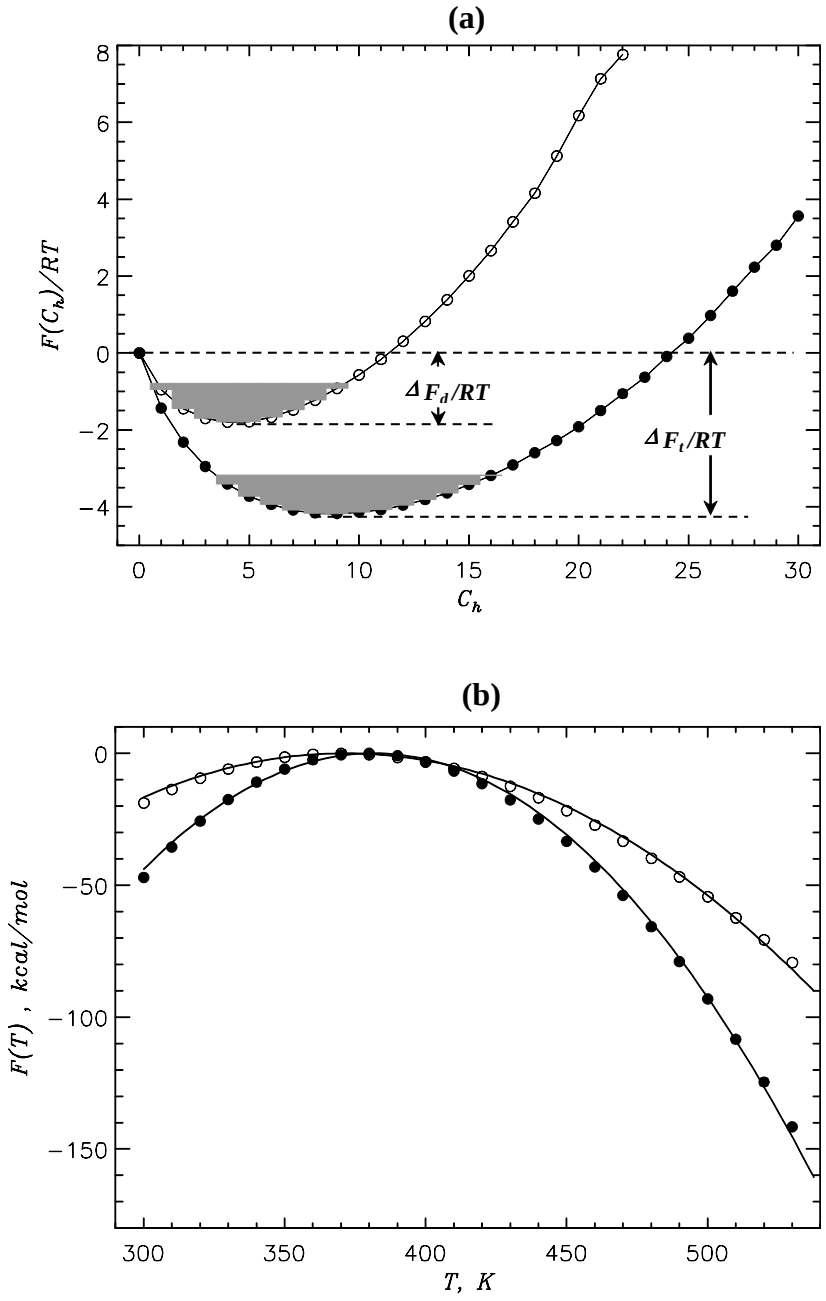

Figure 6 *(a) Free energy of oligomerization with respect to the number of hydrophobic contacts C_h. (b) System free energy as a function of temperature. Open and filled circles represent data for dimer and tetramer, respectively.*

In **Figure 7a** we plot the normalized radial number density $g(r)$ of heavy atoms for the oligomers at 360 K. We observe that for both dimer and tetramer, there is a core region, where the number density is nearly constant, and a surface region, where there is a sharp decrease in the density. **Figure 7b** shows the functions $g(r)$ for tetramers for the temperature range 330-490 K. Since all curves have the inflection points near $r \sim 15$ Å, we infer that as temperature decreases, there is a redistribution of atoms from the surface layer to the core region and shrinkage of the surface layer.

To make this connection clearer, we plot in **Figure 8a** the core radius and surface thickness for dimer and tetramer against temperature. We see that for both oligomers, the core radius is almost constant in the entire temperature range. On the other hand, the surface thickness increases with temperature. On the other hand, in **Figure 8b** we plot the average number density of atoms in the core region n_c as a function of temperature. For both oligomers, n_c increases as temperature decreases. Since the core radius is almost constant, we conclude that atoms are "pumped" into the core as temperature decreases**.** **Figure 8c** plots the fraction of atoms in the core region $\Phi_c(T)$ at each temperature. We see that at $T_c \sim 370$ K, half of the atoms is in the core region, which agrees with T_o computed from the system free energy (**Figure 6b**).

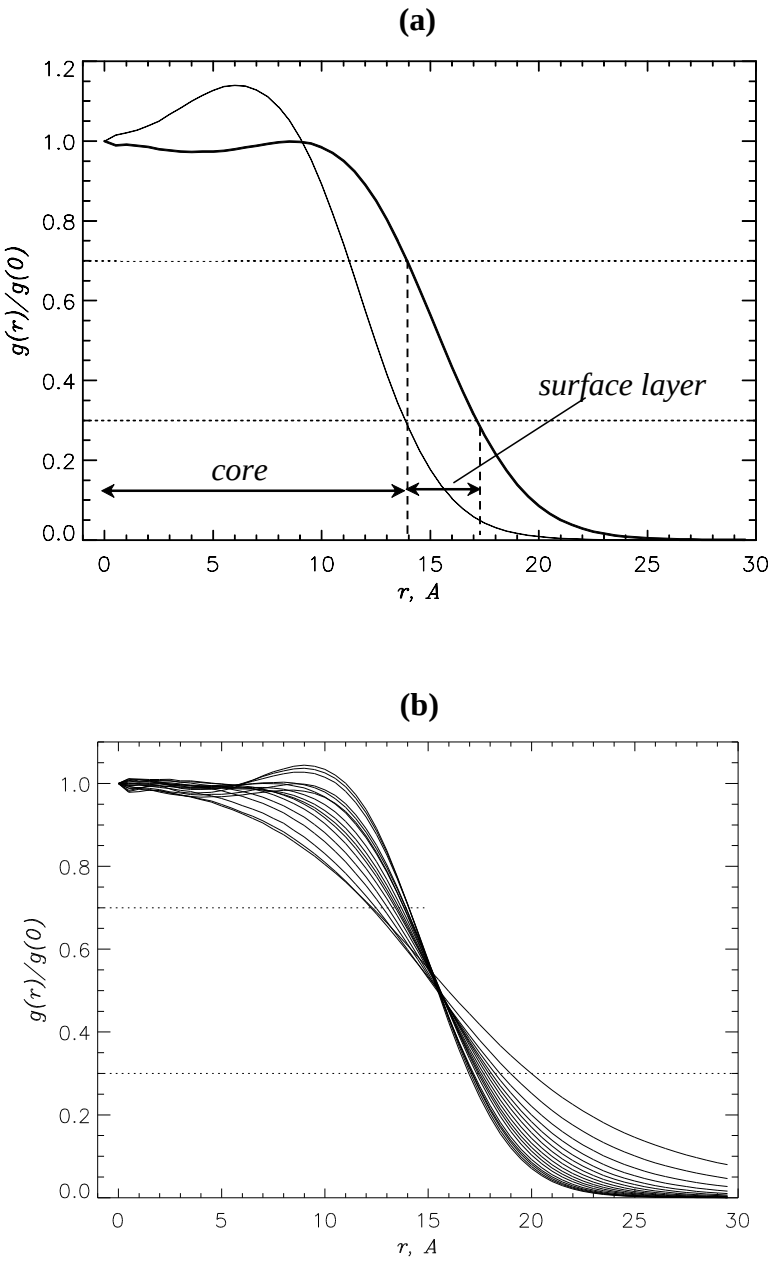

Figure 7 *(a) Normalized radial number density function for heavy atoms g(r) for dimer (gray) and tetramer (black). Operationally, we define the core and surface regions using the radii R_c and R_s, defined as $g(R_c) = 0.7g(0)$ and $g(R_s) = 0.3g(0)$. Then the surface thickness is R_s-R_c. (b) g(r) for tetramer in the temperature range from 330 K to 490 K.*

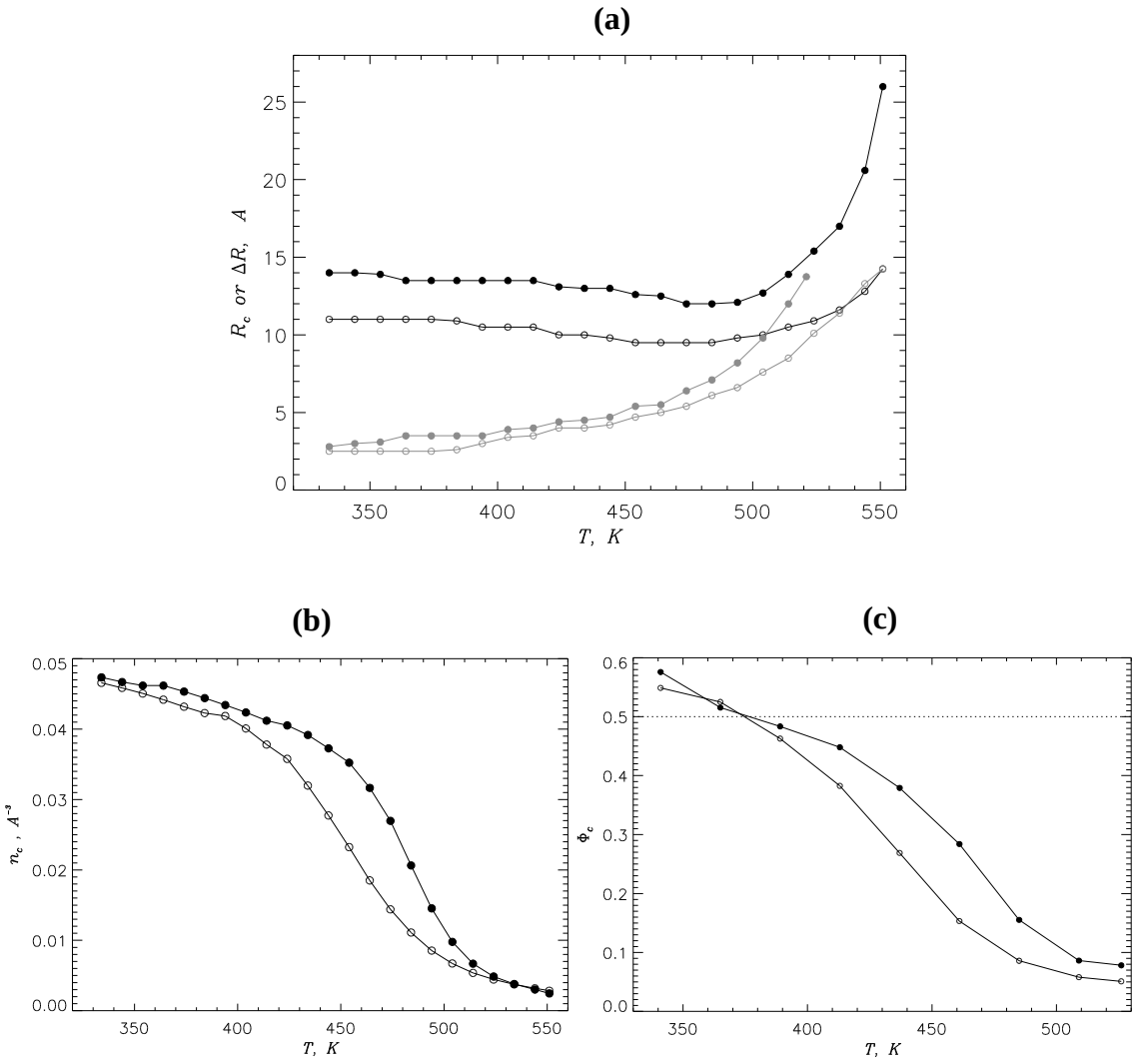

Figure 8 *(a) Core radii for tetramer (filled black) and dimer (open black) and surface thickness for tetramer (filled gray) and dimer (open gray). (b) Atom number density $n_c(T)$ in the core as a function of temperature for tetramer (filled circles) or dimer (open circles). (c) Fraction of oligomer atoms $\Phi_c(T)$ in the core.*

4.1.2 Structure of Aβ oligomers

In order to assess different roles played by amino acids in Aβ oligomerization, we plot in **Figure 9a** the averaged relative solvent assessable surface area < *rASA*(*i*) > per residue. We see that C-terminal (Ct) shows higher solvation than the N-terminal (Nt) with <*rASA*(Ct)>/<*rASA*(Nt)> ~ 1.2 for dimer and 1.3 for tetramer. We also observe that the dimer and tetramer show remarkably similar values of <*rASA*> for all amino acids.

To examine the distribution of residues in oligomers, we plot in **Figure 9b** the probability for each residue to reside in the core region. Again, we see a close agreement between the dimer and tetramer, with N-terminal residues having higher propensity to occur in the core region compared to the C-terminal. The probabilities for Nt and Ct amino acids to occur in the core are 0.59 and 0.33 for tetramer and 0.57 and 0.40 for dimer. We conclude that the oligomer core region is predominantly composed of N-terminal residues.

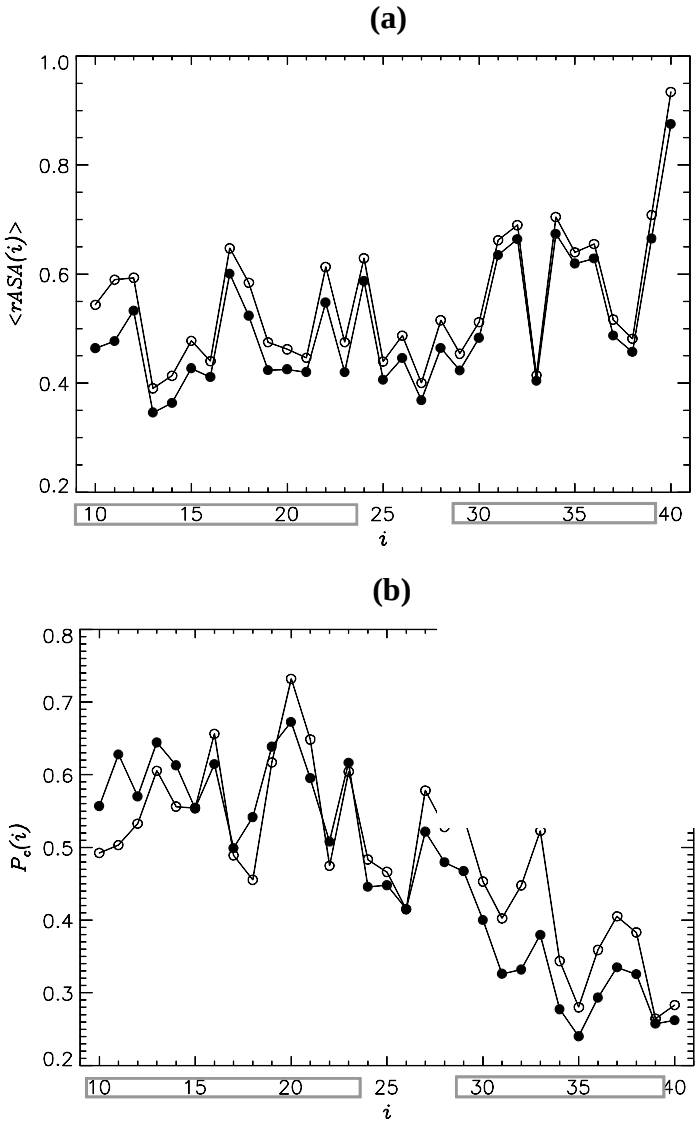

Figure 9 *(a) Relative accessable surface area <rASA(i)> per residue i. (b) Probability of occurrence in the core $P_c(i)$ per residue.Data for tetramer and dimers are shown by filled and open circles, respectively. Nt and Ct terminals are boxed.*

4.1.3 Conformational propensities of Aβ oligomers and monomers

Important insights in oligomerization process can be obtained by computing the distribution of β-strand and helix structure. Indeed, upon monomer to dimer aggregation a remarkable change in secondary structure occurs; the β-strand content $<S>$ (i.e. the fraction of amino acids in β strand conformation) increases from 0.24 to 0.37, while the helix content $<H>$ decreases from 0.32 to 0.21. On the other hand, there is small difference (< 0.02) between dimer and tetramer. In **Figure 10a** we plot the distributions of secondary structure propensities, $<S(i)>$ and $<H(i)>$, along the sequence. Dimer and tetramer show almost identical distributions of secondary structure, while they are profoundly different from those for monomer.

We also computed the distribution of strand and helix lengths, L_s and L_h. The average number of residues occurring in the strand fragment of the length L_s, $<N(L_s)>$, plotted in **Figure 10b** shows that longer strands can be found more often in the dimer and tetramer rather than in the monomer. Again, dimer and tetramer show similarity in strand length distributions, which is different from the distribution for monomer.

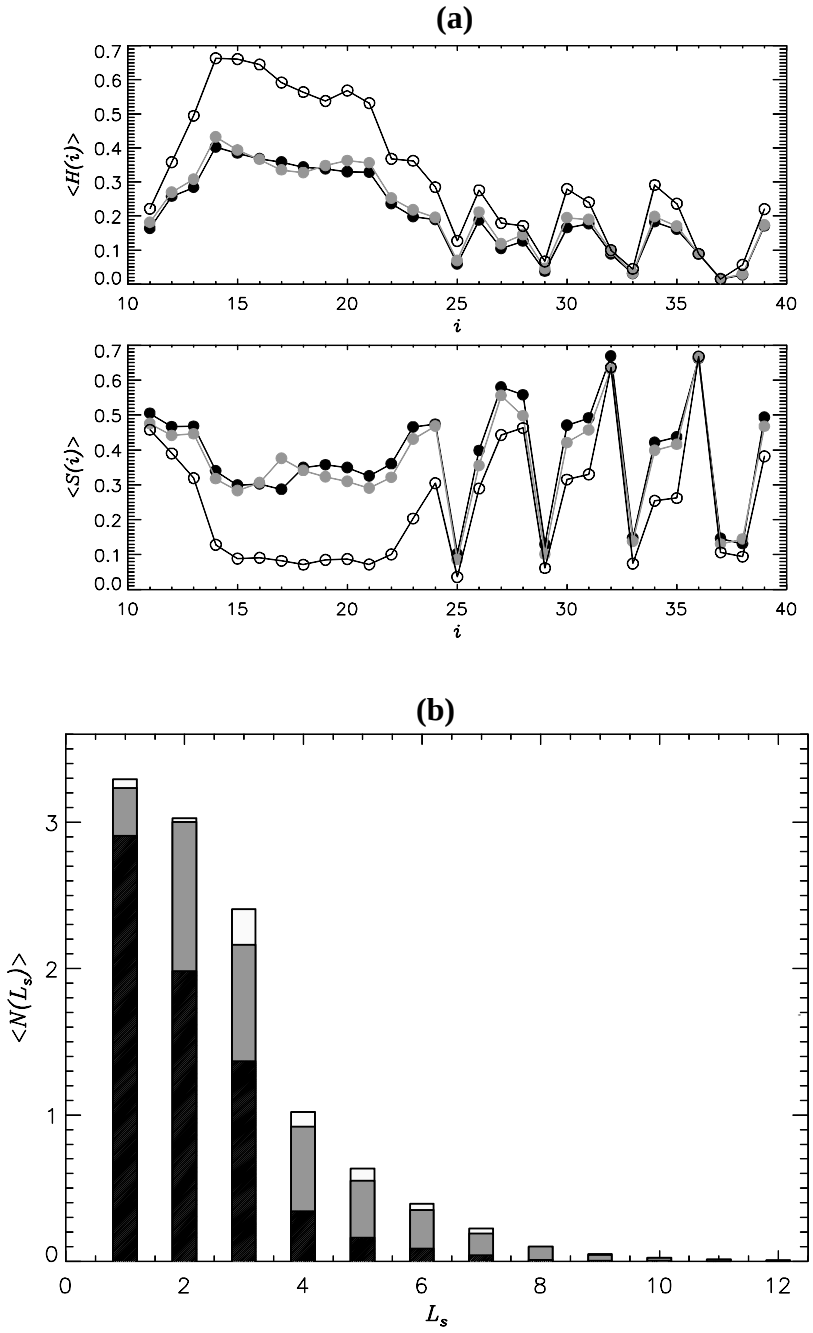

Figure 10 *(a) Propensity per each residue i for forming helix <H(i)> and strand <S(i)> structure. Tetramer, dimer and monomer are shown with filled, gray and open circles, respectively.(b) Number of residues <N(L_s)> involved in the strand of length L_s. Tetramer, dimer and monomer are represented with open, gray and filled bars, respectively.*

Finally, we have computed the free energy landscape $F(S)$ for monomer and oligomers as a function of strand content S (**Figure 11**). We see that there is a flat minimum spanning broad range of strand contents for the dimer and tetramer. Tetramer and dimer have minima of -8.6RT and -7.8RT, so there is only a marginal difference in the values of free energy minimum. On the other hand, monomer shows much higher minimum of -5.6RT at much smaller value of S.

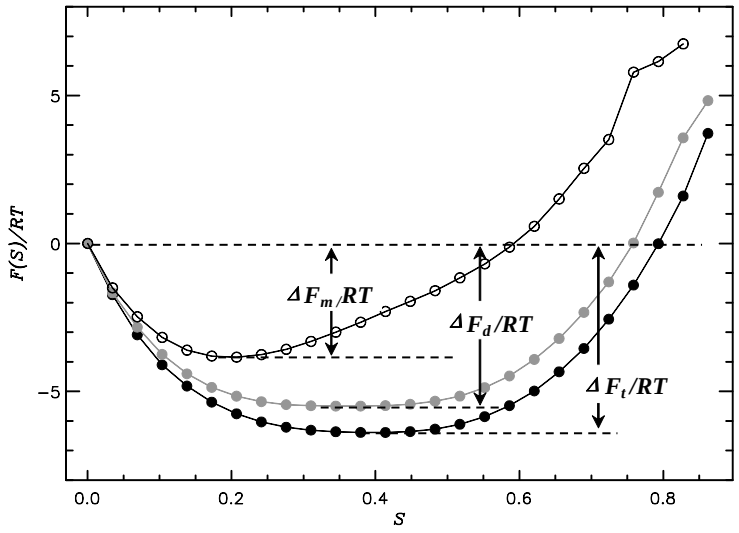

Figure 11 *Free energy landscape F(S) with respect to the strand content S for monomer (open circles), dimer (gray circles) and tetramer (filled circles).*

4.1.4 Conformational clusters of Aβ oligomers and monomers

We used clustering algorithm described in Methods to probe the conformational ensemble of Aβ monomer and oligomers (**Figure 12**). We first describe the tetramer ensemble. The clustering produced three major clusters T1-T3, which together comprise 88% of all structures (**Table 1**). Structures in T1 are characterized by high strand content both in N- and C-terminals, and low helix content (S = 0.46, H = 0.14). This cluster has highest number of interpeptide contacts and lowest number of intrapeptide hydrogen bonds (HB). This cluster T1 is referred to as β-structure cluster. In contrast, structures in T2 have almost equal propensity for strand and helix (S = 0.29, H = 0.30). Compared to T1, structures in T2 have fewer interpeptide contacts and reveal elevated intrapeptide HBs. Cluster T2 is therefore referred to as helical cluster. Cluster T3 resembles T2, but it has lower helix content, especially at Nt. It also has reduced strand content in Ct compared to T1 and T2. T3 has as much intrapeptide interactions as T2, so we refer to the cluster T3 as the collapsed cluster. In all clusters T1-T3, the main aggregation interface is centered at the N-terminal.

Table 1 *Structural clusters in $A\beta_{10\text{-}40}$ tetramer.*

Cluster	p^a	S^b	H^b	C^c	$N_{hb}{}^d$	$N_{ihb}{}^e$
T1	0.46	0.46 (0.48,0.47)	0.14 (0.21,0.09)	60.9 (33.0,16.4)	8.2	5.2
T2	0.23	0.29 (0.16,0.46)	0.30 (0.52,0.10)	51.0 (26.0,16.4)	4.8	10.8
T3	0.19	0.33 (0.37,0.27)	0.23 (0.32,0.19)	52.6 (31.1,11.9)	5.3	10.7

a: Probability of occurrence of each cluster.
b: Fraction of residues in strand (S) or helical (H) conformation. (Those in Nt and Ct are shown in parenthesis).
c: Number of interpeptide contacts.Contributions from Nt and Ct are shown in parenthesis.
d: Number of interpeptide HBs.
e: Number of intrapeptide HBs.

If we consider the conformational clustering of the dimer, we find that the results are similar to the tetramer. We again find three major clusters D1-D3, which together comprise 91% of the structures (**Table 2**). By comparing secondary structure content, interpeptide and intrapeptide interactions, we conclude that D1, D2 and D3 resemble corresponding T1, T2 and T3 clusters for the tetramer, respectively. To be noted is the fact that not just structural quantities, but also the probabilities of occurrences of the clusters are similar for tetramer and dimer. We conclude that Aβ oligomers feature similar conformational ensembles, at least up to tetramer.

Table 2 *Structural clusters in $A\beta_{10\text{-}40}$ dimer. See* ***Table 1*** *for explanation.*

Cluster	*p*	*S*	*H*	*C*	N_{hb}	N_{ihb}
D1	0.47	0.44 (0.46,0.45)	0.15 (0.22,0.09)	33.1 (17.5,9.5)	4.7	6.9
D2	0.25	0.27 (0.15,0.42)	0.31 (0.52,0.12)	28.8 (15.3,8.8)	2.9	11.7
D3	0.19	0.29 (0.32,0.23)	0.26 (0.36,0.20)	27.3 (15.5,7.1)	2.7	13.1

When we investigate the conformational clustering of Aβ monomer, we find that the results are quite distinct from those of the oligomers. We find two major clusters, M1-M2, which together represent 88% of the structures (**Table 3**). Cluster M1 resembles D2 and T2 in that it features higher helix content and intrapeptide HBs, so we refer to it as a helix cluster. On the other hand, the cluster M2 resembles none of the major clusters in dimer or tetramer. It has elevated helix structure, lower strand content and highest intrapeptide HBs. Therefore, we refer to it as all-helix cluster. It is also important that the β-structure clusters, T1 and D1, which are the most populous in the tetramer and dimer, are not observed in the monomer. This analysis offers a strong evidence that the conformational properties of Aβ monomers and oligomers are strikingly different.

Table 3 *Structural clusters in $A\beta_{10\text{-}40}$ monomer. See* ***Table 1*** *for explanation.*

Cluster	*p*	*S*	*H*	N_{ihb}
M1	0.55	0.26 (0.16,0.35)	0.31 (0.52,0.15)	12.9
M2	0.33	0.17 (0.13,0.24)	0.37 (0.54,0.21)	17.4

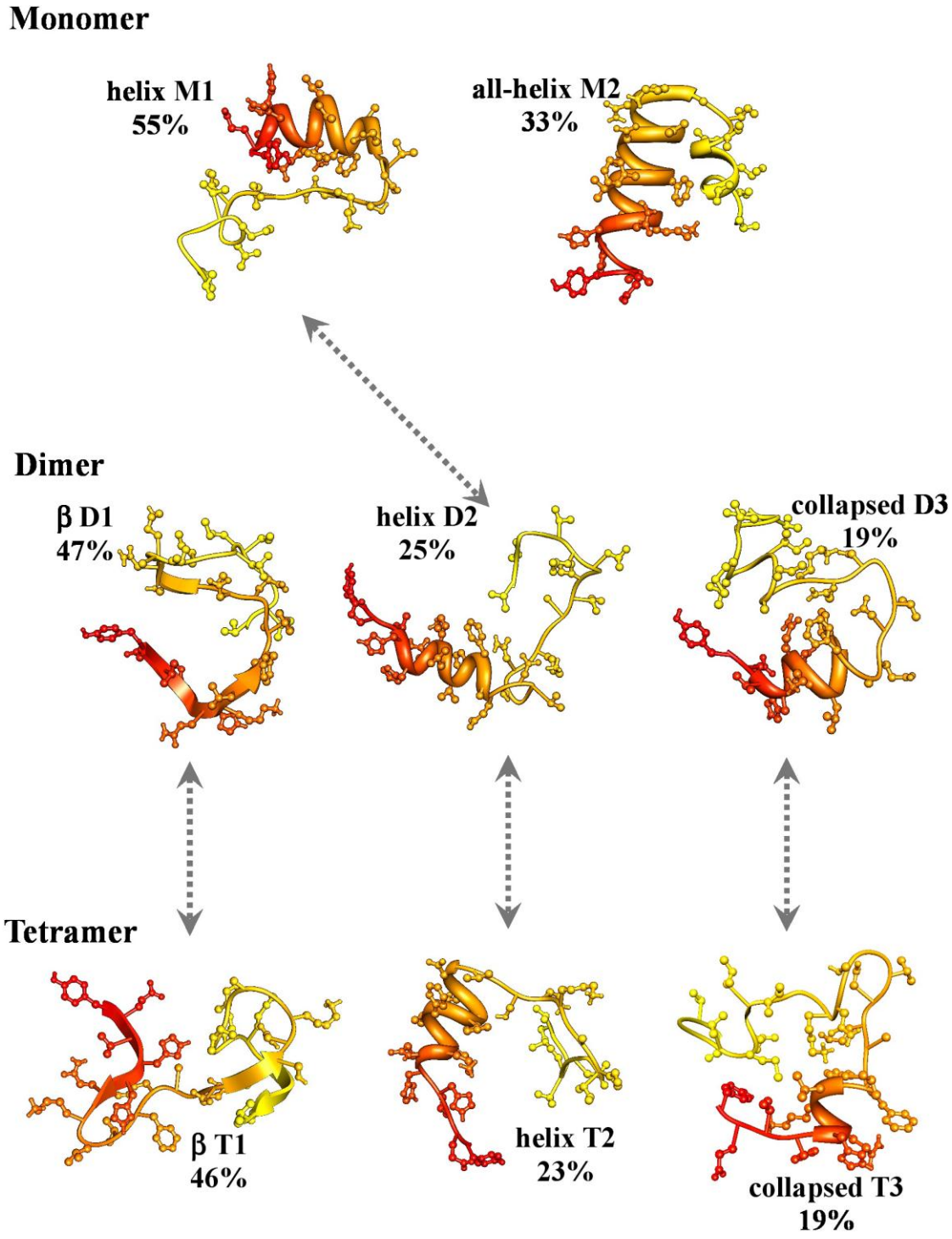

Figure 12 *Representative structures of conformational clusters for Aβ tetramer (T1-T3), dimer (D1-D3) and monomer (M1-M2).*

4.2 Discussion

4.2.1 Aβ oligomerization is a continuous process

Our REMD simulations suggest that Aβ oligomerization is a continuous, barrierless process. Indeed, the free energy plot as a function of the number of interpeptide hydrophobic contacts C_h shows no metastable states. Also, consistent with the thermodynamics of continuous phase transitions, the system free energy as a function of temperature T shows quadratic behavior for $T < T_o$, where T_o is the oligomerization temperature [62].

This continuous nature of oligomerization is also consistent with the atom density distribution of the oligimer. **Figure 7** shows that the oligomer can be characterized by a globular structure comprised of a core region, where the atom density profile is approximately constant, and the surface layer, where the density decreases quickly. Over the temperature range of stable oligomerization, the core region has nearly constant volume, while the surface layer volume decreases with the temperature. Atom number density n_c plot for different temperatures (**Figure 8**) shows that as temperature decreases, atoms are pumped into the core region, resulting in a steady increase in the core atom density.

Such density distribution and its dependence on temperature bear strong resemblance of those for polymer globule near globule-coil transitions. According to polymer theory, the globule-coil transition is continuous and barrierless [63].

4.2.2 Structural properties of Aβ dimers and tetramers are similar

Our result shows that the structural properties of Aβ dimer and tetramer are similar. They both exhibit globular states, which consist of the core and surface region. In **Figure 8** we showed that the atom density profiles of the core region for $T < 400$ K are similar for both species. The thicknesses of surface layers are also similar, as are the temperatures of oligomerization T_o (only ~ 10 K difference in **Figure 6**). Also, the plot of accessible surface area shows little difference for dimer and tetramer (**Figure 9a**). In both species, the core region is mainly composed of the N-terminal, while the C-terminal mainly comprises the surface region with elevated exposure to the solvent.

4.2.3 Conformations of Aβ peptides in dimers and tetramers are similar

The peptides in dimers and tetramers form similar amount of intrapeptide interactions. For example, the ratio of interpeptide interactions formed by Nt and Ct, $\langle C(Nt)\rangle/\langle C(Ct)\rangle$ is similar for dimer and tetramer (about 2 at 360 K). Therefore, in both dimer and tetramer, Nt has about twice as much interpeptide interactions compared to the Ct, forming the main interface of aggregation.

The distributions of secondary structure in the dimer and tetramer peptides shown in **Figure 10** are very similar for both species. Free energy profiles as a function of strand content also show similar behavior (**Figure 11**), with marginally lower minimum for tetramer than for dimer.

Conformational clustering shows most compelling evidence of similarity between the conformational ensembles of dimer and tetramer. Both species are represented by three major clusters, which are similar to each other both structurally and via the probability of occurrence (**Figure 12** and **Tables 1-2**). We conclude that the conformations of small Aβ oligomers are independent of oligomer order, at least up to tetramers.

4.2.4 Conformations of Aβ peptides in oligomers and monomers are distinct

Compared to the oligomers, Aβ monomer exhibits about 80% higher number of intrapeptide HBs and 25% higher number of side-chain contacts. The distribution of secondary structure of monomer shows striking difference compared to oligomers. The fractions of strand and helix structure in the tetramer, for example, are 40% higher and 60% lower than in the monomer. Free energy of the strand structure in the monomer is 3.0*RT* higher than in the tetramer (**Figure 11**)

Conformational clustering also shows difference between monomers and oligomers. Among two major clusters for the monomer, the helix cluster M1 is similar to D2 or T2, while a significant fraction of structures (30%) forms an all-helix cluster M2, which is not seen in the oligomers (**Figure 12**). Conversely, clusters with high strand content (> 0.3) observed in the oligomers (D1, D3, T1, T3) do not appear in the monomer conformations.

In summary, the change in the conformation of monomer via oligomerization can be characterized by the loss of intrapeptide interaction, disappearance of all-helix cluster and emergence of conformations with elevated strand content.

4.2.5 Comparison with experiments

Recently, experiments have been conducted using photoinduced chemical crosslinking technique to probe the Aβ aggregated species [11]. The CD analysis of the secondary structure can be compared with the results of present study and those on Aβ fibrils employing the same simulation methods [60]. The in-silico β-strand contents of Aβ monomer, dimer, tetramer and fibril observed in our simulations and in [60] were: 0.24, 0.37, 0.39 and 0.52, respectively. They are in remarkable agreement with the experimental results for the same quantities: 0.24, 0.39, 0.45 and 0.47. In experiments and simulations, the β-strand contents significantly increases upon monomer to dimer transition (~ 60%), while the increase is much less profound upon dimer to tetramer transition (~ 15%).

4.3 Conclusion

We studied the Aβ monomer and oligomers in aqueous environment using REMD and implicit solvent model. We found that for dimer and tetramer, oligomerization process is continuous without barriers. Typical features of globular structure consisting of core and surface regions emerge for both species, which also exhibit common aggregation interface consisting of the N-terminal. Solvent exposure and secondary structure preferences of each amino acid demonstrate that dimers and tetramers share similar structural properties. However, they are profoundly different when monomer and oligomers are compared. Clustering of conformational ensembles also show that significant structural transition occurs upon monomer to dimer aggregation, while dimer to tetramer conversion largely preserves those ensembles.

5. Aβ DIMER COINCUBATED WITH NAPROXEN

5.1 Results

5.1.1 Naproxen destabilizes Aβ dimer

We plot the number of interpeptide contacts $<C(T)>$ and the number of interpeptide hydrophobic contacts $<C_h(T)>$ as a function of T for the Aβ dimers in water and in naproxen solution in **Figure 13a**. At 360 K the number of interpeptide side chain contacts is $\underset{\sim}{}$ 19.8 in naproxen solution, compared to $\underset{\sim}{}$ 30.0 in water. These computations indicate that about a one third of Aβ interpeptide interaction is lost in naproxen solution. Moreover, since $<C(T)>$ declines with decreasing T for T < 400 K, the antiaggregation effect of naproxen seems to increase with decreasing temperature.

We can also probe the destabilizing effect of naproxen using the free energy profile $F(C)$ as a function of the number of interpeptide contacts C (**Figure 13b**). Aβ dimer in naproxen solution, as well as in water, shows single minimum in the free energy profile, suggesting that the dimerization is a barrierless, continuous process. When we consider the free energy minima, we obtain -6.1RT in naproxen solution compared to -7.5RT in water. So naproxen reduces the free energy gain of dimerization by about 1.4RT.

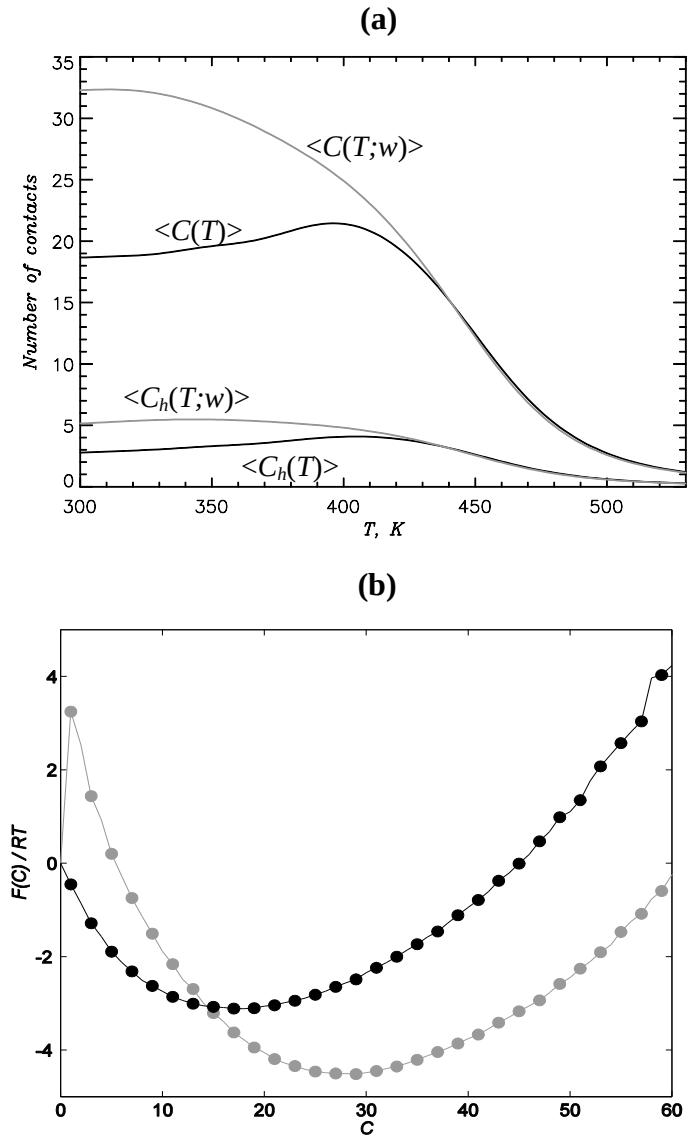

Figure 13 *(a) Numbers of interpeptide side chain contacts <C(T)> or hydrophobic contacts <C_h(T)> in Aβ dimer in ligand free (gray) and naproxen solutions (black). (b) Free energy profile of Aβ dimer in water (gray) and in naproxen solution (black) as a function of the number C of interpeptide contacts at T=360K. The free energy of unbound state (C=0) is set to be zero for both systems.*

To investigate the structural properties of the globular states, we plot in **Figure 14a** the radial number density $g(r)$ as in Chapter 4. As in water, $g(r)$ for Aβ dimer in naproxen solution exhibits a core region, in which the number density is approximately constant, and a surface layer, where the density sharply decreases. At 360 K, the core radius R_c = 12 Å, where R_c is defined as in **Figure 7a**. In **Figure 14b** are shown the core volumes against temperature in ligand free water and in naproxen solution. We see that for T < 400 K, Aβ coincubated with naproxen has greater core volume V_c, which shows more expansion as temperature decreases. For example, V_c is about 30% larger in naproxen solution at 360 K. To investigate this phenomenon closer, we plot in **Figure 14c** the $\Phi_c(T)$ which is the fraction of atoms in core. We see that there is little difference of $\Phi_c(T)$ in water or in naproxen solution. However, the plot of $n_c(T)$ in **Figure 14d**, the average peptide atom number density in core, shows that there is a considerable difference in water and in naproxen solution. We also see that the naproxen atom number density $n_c(npxn)$ increases with decreasing temperature, resulting in influx of naproxen into dimer volume. **Figure 14c** demonstrates that the fraction of naproxen atoms $\Phi_c(npxn)$ ~ 0.32 penetrate into the dimer core at 360 K.

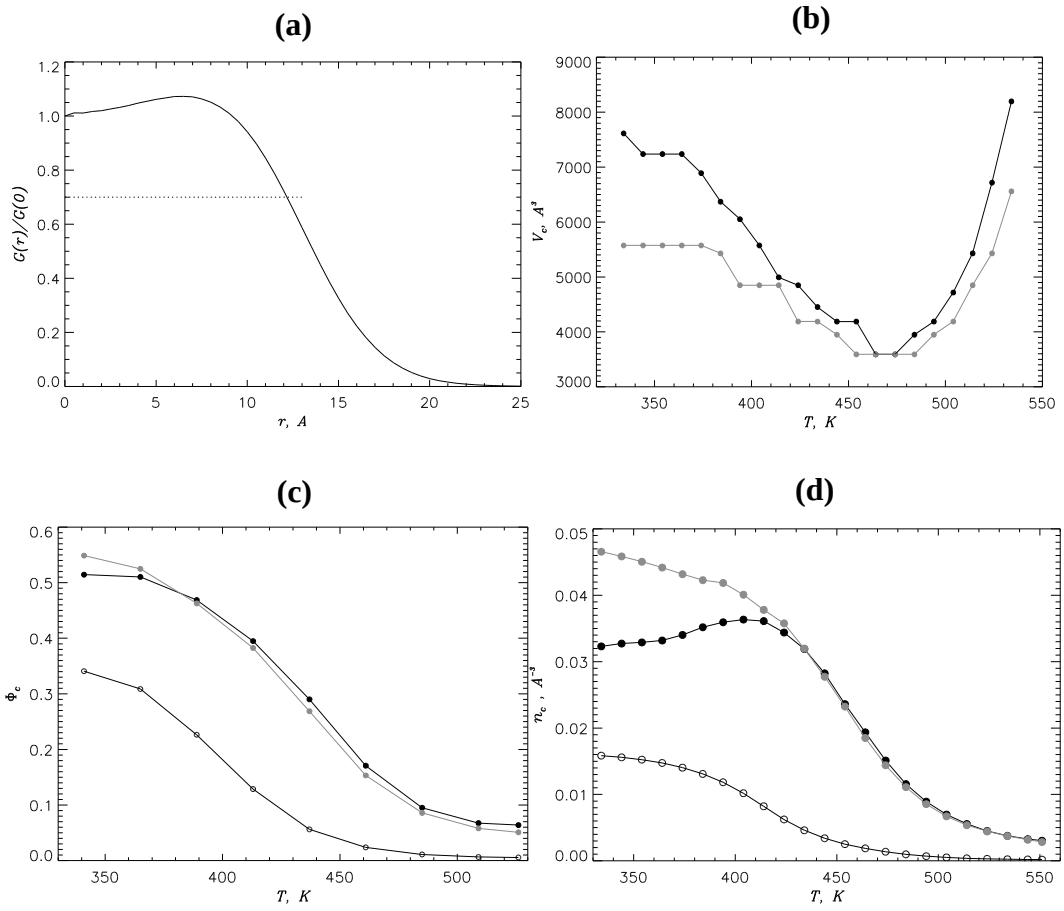

Figure 14 *(a) Normalized radial number density function g(r) for heavy atoms of Aβ dimer at 360 K. (b) Core volumes $V_c(T)$ of Aβ dimer in water (gray) and in naproxen solution (black). (c) The fraction of Aβ or ligand atoms in the core $\Phi_c(T)$ in water (gray) and naproxen solution (black). The fraction of naproxen atoms in the core n_c(npxn) is shown by open circles. (d) Atom number density of Aβ dimer or naproxen in the core $n_c(T)$ using the same scheme of representation as in (c).*

We also computed the interpeptide contact maps $\langle C(i,j) \rangle$, which present the average number of contacts between residues *i* and *j* in the Aβ dimer in naproxen solution or ligand-free water. Based on these computations, in **Figure 15a** we plot the difference

contact map $<\Delta C(i,j)>$, which shows the changes in probabilities of interpeptide contact due to the presence of naproxen. It is shown that naproxen causes either the reduction of contact probability or leaves it intact. The impact on the contact probability is observed both at N- and C-terminals, which reveal about 32% and 38% decrease, respectively. The most impacted are the residues Phe20, Phe19 and Tyr10. However, naproxen does not change the aggregation interface, as indicated in **Figure 15b**. The average number of interpeptide contacts $<C>$ in Nt and Ct are 11.0 and 5.3 in naproxen solution, while the corresponding quantities are 16.1 and 8.6 in water, respectively. Hence, both in water and in naproxen solution the main aggregation interface is located at the N-terminal. We also compared the probability $P_c(i)$ of occurrence in the core region of each residue. We find that the distribution is similar for water and naproxen solution; the average probabilities within Nt and Ct are 0.57 and 0.35 in naproxen solution, while they are 0.57 and 0.40 in water. So in both cases the Nt is typically buried in the dimer core, while Ct is exposed to the solvent. We also computed the secondary structure of Aβ dimer in naproxen solution, but found that it is hardly affected compared to the dimer in water.

(a)

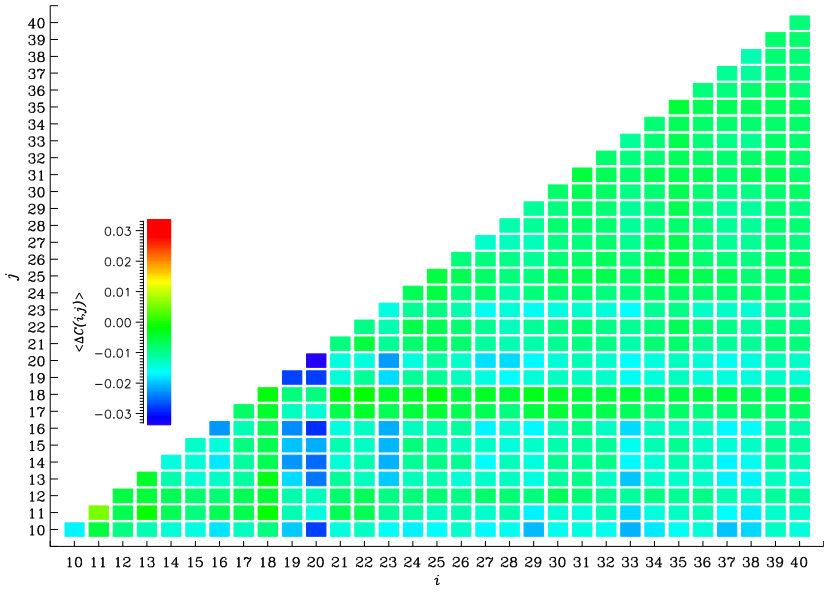

(b)

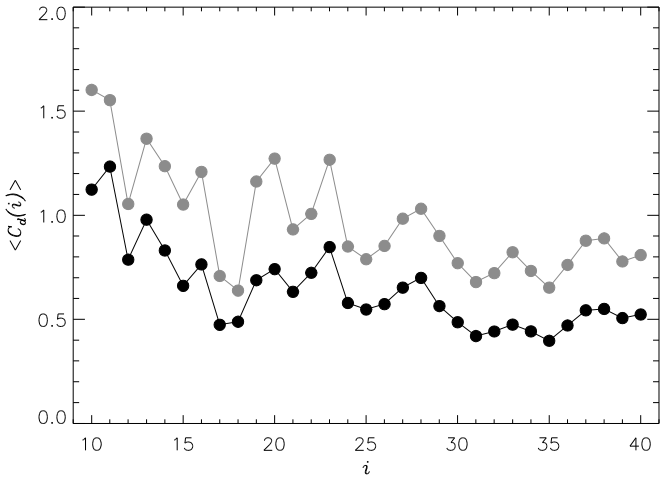

Figure 15 *(a) Difference interpeptide contact map <ΔC(i,j)> for Aβ dimer. (b) Number of interpeptide contacts per residue for Aβ dimer in water (gray) and in naproxen solution (black).*

5.1.2 Naproxen binding to Aβ dimer affects interpeptide interaction

To assess destabilizing effect of naproxen on Aβ dimer, we computed the probability of naproxen binding P_b to the dimer. At 360 K, $P_b \sim 0.71$, so the average number of bound naproxen molecules $<L>$ is about 14.2. We also computed the average number of naproxen molecules $<L_i>$ that bind both peptides in the dimer simultaneously, i.e. those that interfere with dimerization. We found that $<L_i> \sim 6.3$, that is, about 45% of the number of bound ligands. Since the total number of contacts between peptides and ligands $<C_l> \sim 58.8$, we see that each bound naproxen interacts with about 4 amino acids.

We also plot the free energy profile of naproxen binding to Aβ dimer as the function of the distance between ligand and dimer (**Figure 16a**). The plot shows a single minimum at about 5 Å, at which the free energy of binding $\Delta F_b = F_{min} - F(r \rightarrow \infty)$ is $-6.8RT$. In order to illustrate the competition between peptide-peptide interaction and peptide-ligand interaction, we plot in **Figure 16b** the radial distribution functions $g_{pp}(r)$ and $g_{pl}(r)$. Here, $g_{pp}(r)$ and $g_{pl}(r)$ map the minimum distances between amino acids from different peptides and the minimum distances between ligands and amino acids, respectively. From the plot of $g_{pp}(r)$ in water, we see that the peak occurs at ~ 5 Å. On the other hand, the corresponding plot for naproxen solution shows reduced peak at about the same location (~ 5 Å) and extended tail toward larger values of r. The plot for $g_{pl}(r)$ shows that the peak also occurs at $r \sim 5$ Å, which coincides with the peak of $g_{pp}(r)$. We conclude that a direct competition between peptide-peptide interaction and peptide-ligand occurs, and that

interpeptide amino acid contacts are suppressed and separation between the peptides grows in the presence of naproxen.

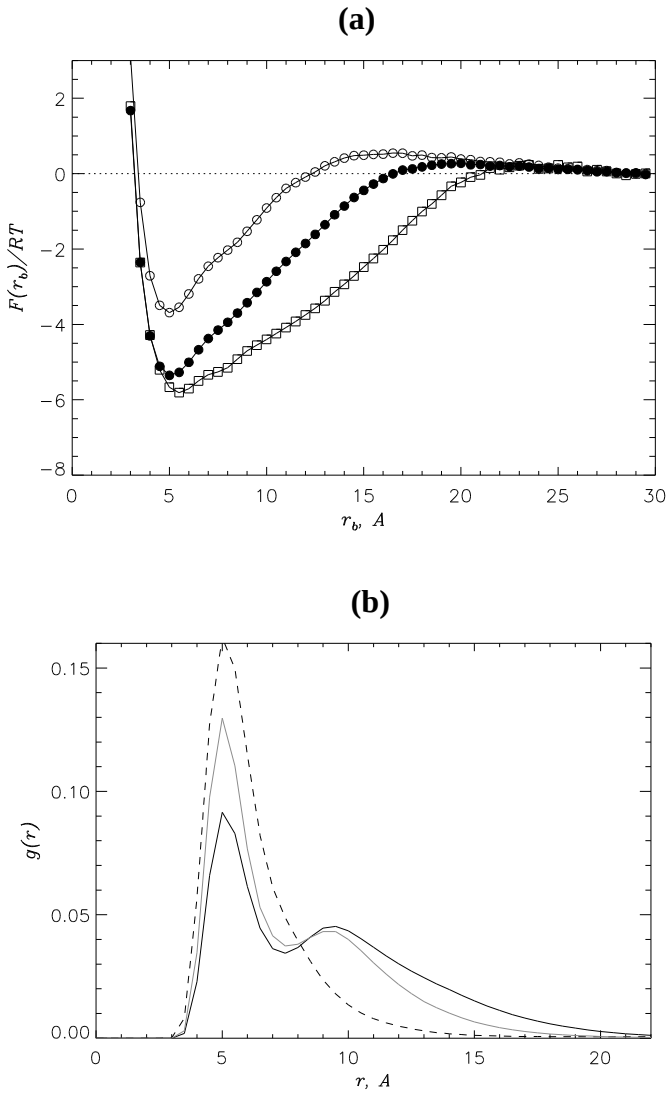

Figure 16 *(a) Free energy profiles of naproxen binding to Aβ monomer (open circles), dimer (filled circles) and fibril (open squares). The fibril data was taken from* [26]. *Data for the monomer are taken from* [25]. *(b) Radial distribution functions $g_{pp}(r)$ for minimum distances between amino acids in water (gray) and naproxen solution (black). Corresponding $g_{lp}(r)$ for peptide-ligand distances is shown with dashed lines.*

5.1.3 Naproxen binding to Aβ dimer is governed by Aβ sequence

In order to probe the factors responsible for Aβ dimer and naproxen interaction, we analyzed the naproxen binding affinities for amino acids from Aβ peptide. **Figure 17** presents the number of contacts $<C_l(i)>$ formed by amino acid *i* with naproxen. Even though there are considerable variations, we see that most interactions with naproxen occur at the N-terminal (the numbers of contacts in Nt and Ct are 19.9 and 8.6, respectively). In **Figure 17** we also plot the interaction energies between amino acid *i* and ligand $<E_b(i)>$. We see that there is a strong correlation between the number of contacts and interaction energy between amino acid and ligand. On the other hand, we found that the secondary structure propensity for each amino acid $<S(i)>$ and $<H(i)>$ are not correlated with the number of ligand contacts $<C_l(i)>$.

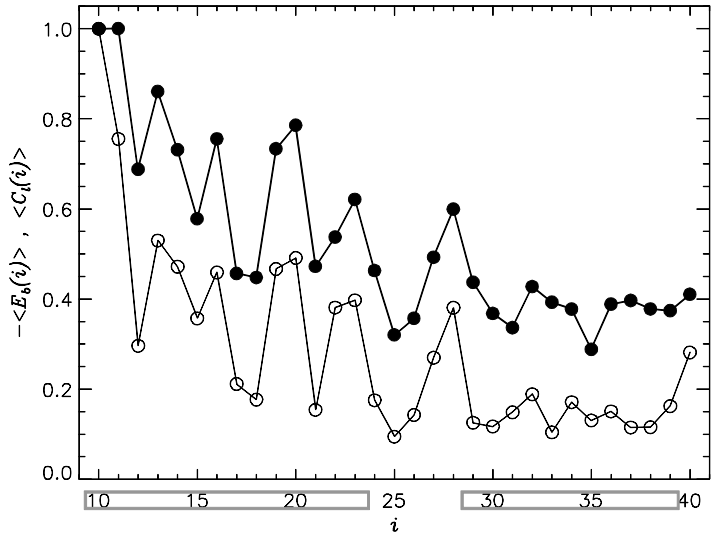

Figure 17 *Number of contacts with naproxen per residue $<C_l(i)>$ (filled circles) and the residue-ligand interaction energy $<E_b(i)>$ (open circles). Nt and Ct terminals are boxed.*

Motivated by earlier study of naproxen interaction with Aβ fibril [25], where interligand interactions make a large contribution to binding energetics, we computed the distribution of size S_c of clusters formed by bound ligands. At 330 K, the distribution is bimodal, where ~ 92% of ligands are incorporated in large clusters (S_c > 6). Average energy of interligand interaction was found to be $\langle E_{ll} \rangle$ ~ -14.7 kcal/mol, while ligand-peptide interaction energy is $\langle E_{lp} \rangle$ ~ -8.0 kcal/mol. Even though the interligand interaction is stronger in magnitude compared to the ligand-peptide interaction, the ligand-peptide binding is more influenced by the latter. Indeed, if we compute these quantities for N- and C-terminals, we find that $\langle E_{ll} \rangle$ shows small difference (~ -1.0 kcal/mol) between Nt and Ct, but the difference in $\langle E_{lp} \rangle$ is ~ -3.3 kcal/mol. This suggests that naproxen binding is mainly driven not by interligand but ligand-peptide interaction, which is a distinct feature compared to naproxen-fibril interactions [25].

5.2 Discussion

5.2.1 Mechanism of naproxen antiaggregation effect

We analyzed the binding of naproxen to Aβ dimer. We found that naproxen binds to the dimer at the temperatures T < 380 K. Naproxen binding destabilizes but does not depolymerize Aβ dimer. Due to naproxen binding, about 1/3 of interpeptide interaction in the dimer is lost. Naproxen binding reduces the free energy gain of dimerization from -7.5RT to -6.1RT. About 1/3 of naproxen molecules penetrate into the dimer core, resulting in about 30% swelling of the core volume. This results in about 25% drop of peptide atom density in the core, compared to water. Among the bound ligands, about 45% are at the dimer interface, competing with peptide-peptide interactions. The free energy of naproxen binding to Aβ monomer was reported in [25] to be -5.1RT. Since the free energy of dimerization in water is -7.5RT, an Aβ monomer is more likely to bind another Aβ chain than naproxen. So naproxen only destabilizes but does not depolymerize Aβ oligomers.

We can also compare the change in free energy of fibrillation and oligomerization in water and in naproxen solution. The free energy gain for Aβ peptide binding to the fibril is -9.9RT in water and -4.7RT in naproxen solution [24], i.e. a reduction in free energy of 5.2RT occurs due to naproxen. On the other hand, the free energy of dimerization is -7.5RT in water and is -6.1RT in naproxen, i.e. naproxen reduces it by 1.4RT. Hence in naproxen solution, Aβ monomer is more prone to oligomerization than fibrillation. We also note that the free energy of naproxen binding to Aβ monomer is -5.1RT [25],

compared to its fibril binding free energy -7.6*RT* [23]. Also, the loss of interpeptide side chain contact via naproxen is 14.9 for fibril [24], but 10.2 for dimer. Taking these observations together, we conclude that naproxen has better antiaggregation effect against fibrils than oligomers.

We observe that naproxen binding does not alter the aggregation interface in Aβ dimer. The aggregation interface is mainly composed of Nt terminal, which is responsible for about 2/3 of interpeptide interaction. Also, the probability of occurring in the dimer core $P_c(i)$ for each amino acid is similar for both water and naproxen solution (not shown). So the dimer core is mainly formed by the N-terminal, while the surface is formed by the C-terminal. We also considered the conformational clusters and secondary structures formed by Aβ dimers in naproxen solution, and found that they show little difference compared to the aqueous environment. In contrast, according to previous studies naproxen induces noticeable change in Aβ monomer conformation, resulting in the increase of strand content by 50% and reduction of helix content by a third [24].

5.2.2 Naproxen binds to Aβ dimers and fibrils via different mechanisms

The mechanism of naproxen binding to the Aβ fibrils has been studied previously [25]. It was found that the ligands exhibit strong interligand interactions while binding to the fibril. The ligand-ligand interaction energy $<E_{ll}>$ was about twice as strong as the ligand-peptide interaction energy $<E_{lp}>$. Also, about 92% of ligands form large (≥6) clusters

bound to Aβ fibrils. In this work, we demonstrated that these features are also shared by the naproxen ligands interacting with Aβ dimers.

However, there are noticeable differences between naproxen interacting with Aβ fibrils and with dimers. For naproxen-fibril interactions, the main factor determining the ligand binding was the geometry of Aβ fibrils. It was found that the naproxen molecules favor the concave (CV) edge rather than convex (CX) fibril edge. Even though the ligand-peptide interaction energy was similar for both cases, the ligand-ligand interaction energy was about 5.5 kcal/mol lower for the ligands interacting with CV edge compared to the CX edge, due to the confinement effect of the former.

In contrast, for the naproxen-Aβ dimer interaction, the ligand-amino acid interactions appear to control the binding sites in Aβ dimer. For example, the change in interligand interaction energy $<E_{ll}>$ along Aβ sequence is three times smaller than corresponding variation in ligand-peptide interaction energy $<E_{lp}>$. Also, as **Figure 16** shows, the distribution of ligand binding sites is strongly correlated to the ligand-amino acid interaction energy. These observations imply that the naproxen binding site in Aβ dimer is determined by the amino acid sequence. Even though the strong interligand interaction is a common feature of naproxen interacting with Aβ fibril or dimer, the determination of binding sites and therefore the binding mechanism are different.

5.2.3 Comparison with experiments

Currently, experiments investigating naproxen interacting with Aβ oligomers are unavailable. However, there are results on molecules that share important structural motifs with naproxen. For example, the effect of curcumin, which has two phenyl rings, on Aβ aggregation has been studied [64]. It was shown that curcumin completely blocks Aβ oligomerization at the ligand to peptide stoichiometric ratio of 3:1. Curcumin also reduces, but does not prevent, fibril formation. Furthermore, curcumin inhibits Aβ cytotoxicity at the stoichiometric ratio of 10:1. Based on the concentrations of curcumin and naproxen required to achieve the same antiaggregation effect, naproxen was found to be four times less potent antiaggregation agent than curcumin. This relative inefficiency of naproxen can be attributed to its weaker antiaggregation effect against Aβ oiligomers compared to that against Aβ fibrils. Since Aβ oligomers are the primary cytotoxic species, we conclude that naproxen has limited efficiency as prophylactic agent against AD.

5.3 Conclusion

We studied the antiaggregation effect of naproxen upon Aβ dimer and compared it with previous results on naproxen interaction with Aβ monomer and fibrils. It was found that naproxen destabilizes Aβ dimer by interfering with aggregation interface. Globular structure of the dimer becomes swollen due to significant penetration of naproxen molecules into the dimer core. Location of naproxen binding sites in Aβ dimer is largely dictated by amino acid composition, unlike the binding of naproxen to Aβ fibrils. Free energy estimates show that naproxen acts as a better antiaggregation agent against fibrils rather than against oligomers, thus compromising its potential as therapeutic agent against AD.

6. INTERACTION OF Aβ MONOMER WITH LIPID MONOLAYER

6.1 Results

6.1.1 Binding of Aβ to lipid monolayer

We studied Aβ monomer and DMPC monolayer system using Charmm19+SASA implicit solvent model. At 360 K, the probability of Aβ monomer binding to DMPC monolayer is ~ 1. Average number of contacts between an amino acid and monolayer is 2.6. The residues in Nt and Ct, on average, form 2.7 and 2.3 contacts, respectively. In **Figure 18a** we plot average number of contacts $<C_{ml}(i)>$ per residue i with the monolayer. We note that the distribution is highly uneven. We define the monolayer binding residues to be those with the number of contacts higher than 80% of the maximum (as shown in the plot). As a result, five residues, Tyr10, His13, Lys16, Phe20 and Lys28, are classified as binding. Importantly, four out of five of them are from the N-terminal, and that they are either aromatic (Tyr10, His13, Phe20) or positively charged (Lys16, Lys28).

To investigate the nature of monolayer binding per residue more closely, we plot in **Figure 18b** the distribution of the centers of mass of each residue along the z-axis. Many residues tend to lie near z ~ 4 Å, which can be attributed to their binding to the monolayer head groups. This observation applies to the binding residues Lys, which

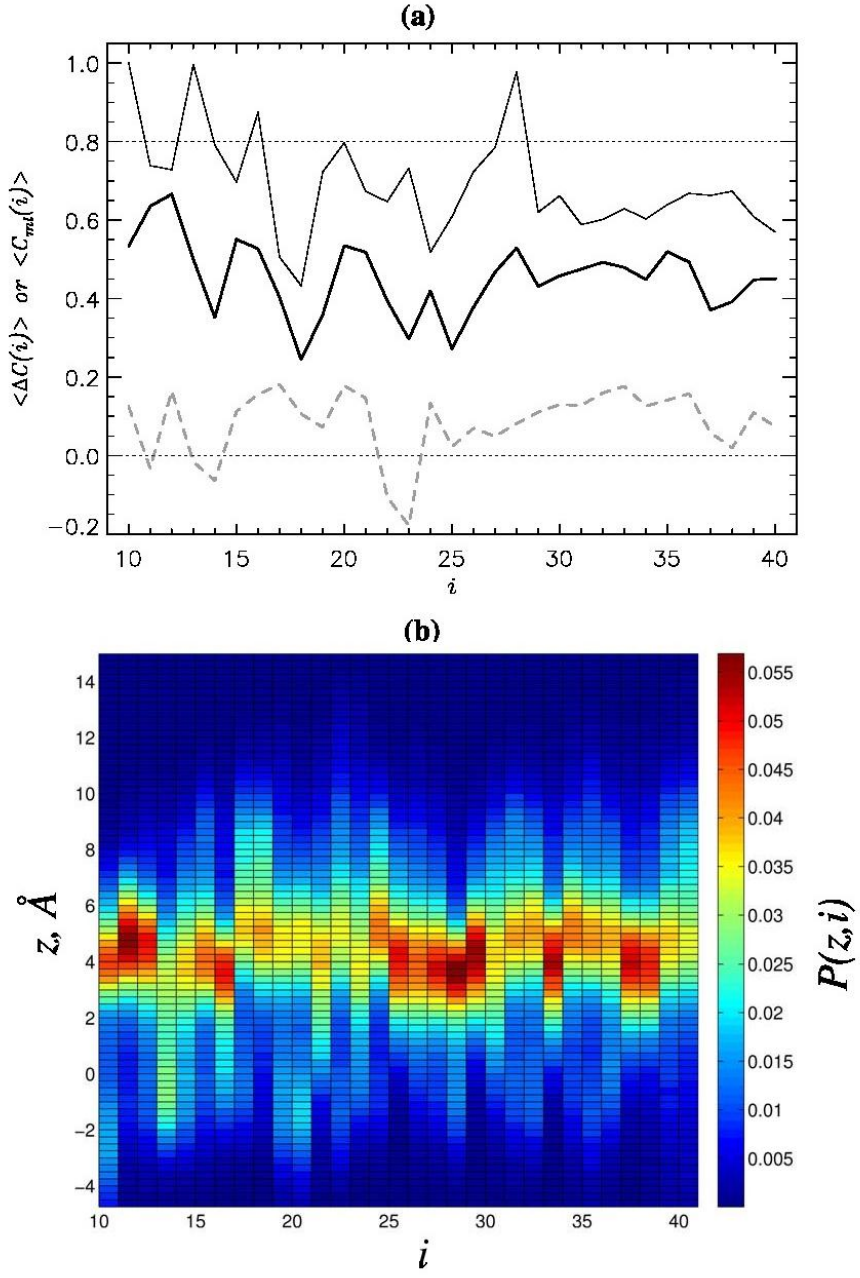

Figure 18 *(a) The number of contacts with DMPC monolayer per residue, <$C_{ml}(i)$>, is shown by thin black line. The normalized difference in the numbers of intrapeptide side chain contacts, <$\Delta C(i)$>=(<C(i;w)>-<C(i;ML)>)/<C(i;w)>, is shown by thick black line. (Here C(i;w) and C(i;ML) denote the numbers of intrapeptide contacts formed by residue i in water and Aβ bound to monolayer, respectively.) The same difference quantity for Aβ dimerization is shown by gray dashed line. (b) Distribution of Aβ side chain i along z-axis, P(z,i).*

largely remain near lipid head group. However, few aromatic residues have second maximum at z < 0 Å, indicating their propensity to penetrate deeper into the core region.

In **Figure 19** we plot the probability for each amino acid to penetrate into the monolayer core region (z < 0 Å). As expected, aromatic residues have highest insertion probability (average of 0.26), but for Lysines the probability of insertion is only 0.13.

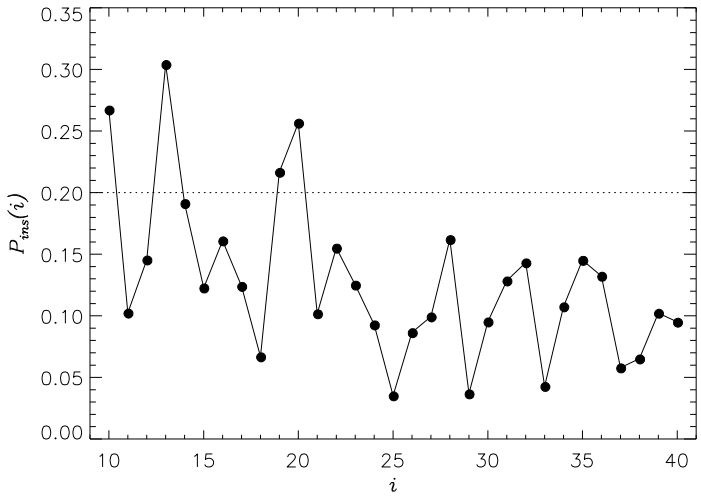

Figure 19 *Probability of occurrence in the core region for amino acids i, $P_{ins}(i)$.*

6.1.2 Impact of monolayer binding on the structure of Aβ

One of the major goals of this research was to elucidate the impact of membrane binding on the structure of Aβ peptide. In order to investigate this question, we computed the average number of intrapeptide contacts in Aβ monomer. Upon monolayer binding, this

value decreases from 32.2 in water to 17.5, indicating about 45% loss of intrapeptide contacts. **Figure 18a** shows the normalized change in intrapeptide contact numbers induced by binding to the monolayer, $< \Delta C(i) >$. We see that the loss in intrapeptide contacts is considerably higher than that observed for Aβ dimerization. So we conclude that monolayer binding has much stronger impact on intrapeptide interaction than dimerization.

Figure 20 shows the distribution of end-to-end distance r_{1N} of Aβ monomer at 360 K. It is clearly shown that the distribution undergoes significant change compared to Aβ in water, resulting in the extension of the peptide upon monolayer binding. Specifically, the average value of $<r_{1N}>$ increases from 18.3 Å in water to 30.7 Å.

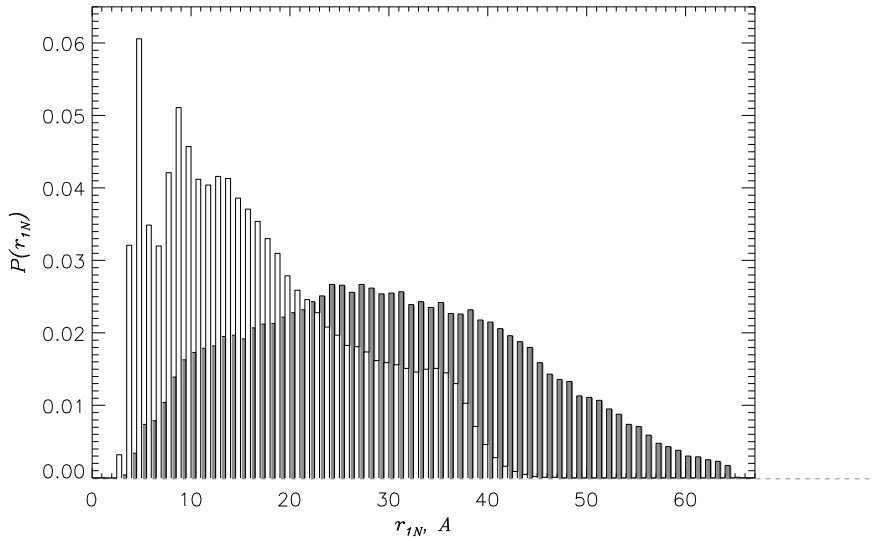

Figure 20 *End-to-end distance distribution of Aβ monomer in water (open bars) or bound to the monolayer (gray bars)*

Finally, we computed the secondary structure content in Aβ monomer bound to the monolayer. In **Figure 21a** we compare the respective distributions along the primary sequence with Aβ monomer in water. It is clear that monolayer binding causes significant increase in β-strand content and decrease in helix content. Specifically, the strand content <*S*> increases from 0.24 to 0.37, while the helix content <*H*> decreases from 0.32 to 0.16 upon monolayer binding. The decrease in <*H*> and increase <*S*> are negatively correlated (the correlation coefficient is -0.84), confirming that the gain in strand structure is responsible for the loss of helix content. This change in secondary structure is more pronounced in the Nt (**Figure 21b**), with helix fraction decreasing from 0.51 to 0.21, compared to Ct where the change is merely from 0.15 to 0.11.

In summary, the interaction with the monolayer causes structural change of Aβ via extension, helix to strand conformational transition, and loss of intrapeptide interaction. This has significant implication for Aβ's cytotoxicity, which is expected to be positively correlated with the enhanced β-strand conformation [18].

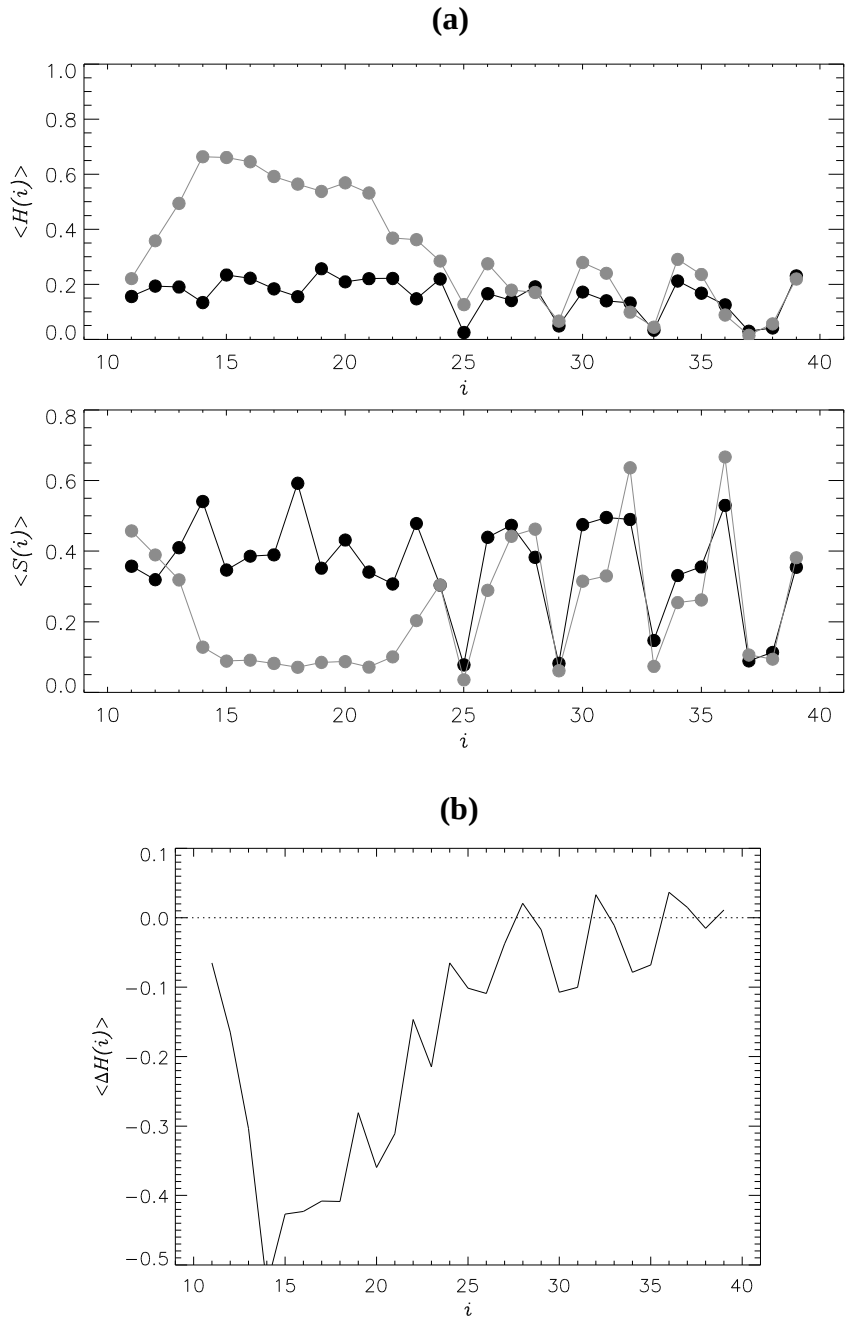

Figure 21 *(a) Secondary structure propensity per residue in Aβ monomer in water (gray) or bound to monolayer (black). (b) Change in helix propensity per residue upon monolayer binding.*

6.1.3 Clustering of the structural ensemble of Aβ monomer

We used clustering algorithm described in Chapter 3 to compute conformational ensemble of Aβ monomer bound to DMPC monolayer. Four major conformational clusters C1-C4 were obtained, which together comprise 99% of all structures. **Figure 22** illustrates each cluster by a representative structure superimposed on the ensembles of backbone conformations. It also shows the contact map of intrapeptide interactions for each cluster. Most populated cluster C1 (55% of structures) consists of conformations with high β-strand (<*S*> = 0.40) and low helix (<*H*> = 0.13) contents. The contact map reveals various close-range interaction with comparable probability. Cluster C2 has the population of 16% and has similar secondary structure propensity as C1, with <*S*> = 0.36 and <*H*> = 0.16. C2 is characterized by the stable Gly33-Gly37 contact occurring with the probability higher than 0.8. As a result this cluster exhibits stronger intrapeptide interactions in Ct. Cluster C3 has the population of 15% with <*S*> = 0.30 and <*H*> = 0.23. It has stable contact Val18-Glu22, which contributes to the highest helix content among all clusters, especially in the N-terminal. Cluster C4 has the population of 13%, with <*S*> = 0.33 and <*H*> = 0.19. It has stable contact Gly25-Gly29, contributing to the turn formation at the residues 24-28. All four clusters reveal higher strand content compared to helical content. We also observe that for all clusters, the N-terminal is the major interaction interface with the monolayer.

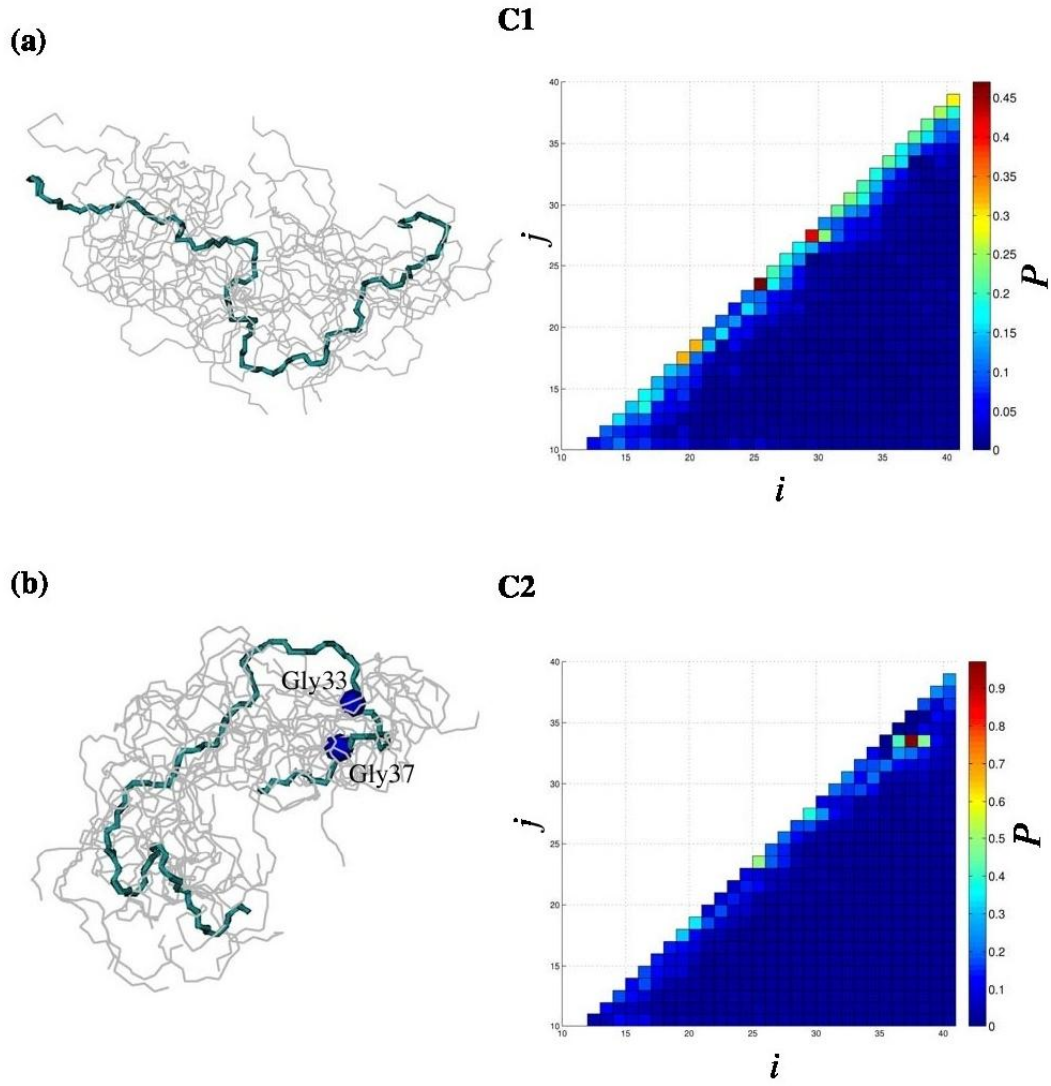

Figure 22 *Major conformational clusters for Aβ monomer bound to the lipid monolayer. Left panels: Representations of major clusters, along with the important side chain contacts. Right panels: intrapeptide contact maps.*

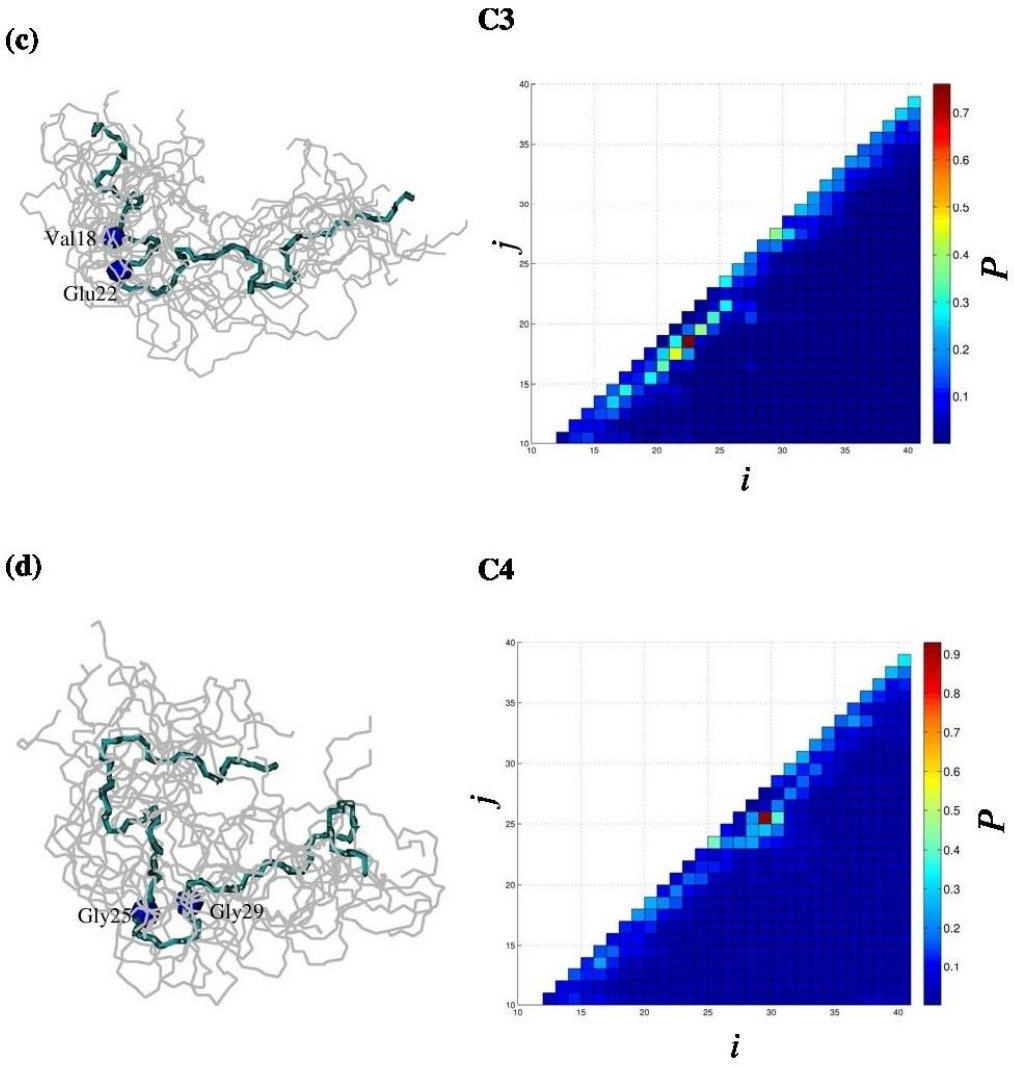

Figure 22 *continued.*

6.1.4 Impact of Aβ binding on the lipid monolayer

To elucidate the role of Aβ peptide in cellular toxicity, it is important to investigate the impact of the Aβ binding on the structure of lipids comprising the membrane. Bevan and others [65, 66] have shown that Aβ interaction causes lipid bilayer thinning, increased disorder, and fluidity. In order to check these results for our model, we computed the local area per lipid as follows. We used two dimensional Delaunay tessellation for the phosphorus P atoms in lipid head groups on the *x*-*y* plane. The area per lipid is defined to be the sum of the areas of triangles sharing the P coordinate as a vertex, divided by 3. The distribution of this quantity is plotted in **Figure 23a**, where the lipids are divided into two groups according their interaction status with Aβ. We see the shift in the distribution, indicating that the area per lipid is decreased due to Aβ interaction from 66 $Å^2$ to 59 $Å^2$.

We also computed the radial pair correlation function $g_{PP}(r)$ for the P atoms in the *x*-*y* plane (**Figure 2**). For a P atom, $g_{PP}(r)$ reports the density of other P atoms at the distance *r*. **Figure 23b** shows the comparison of $g_{PP}(r)$, computed for lipids forming contacts with Aβ or for those in the Aβ-free region. For lipids that are not contacting Aβ, $g_{PP}(r)$ shows oscillating pattern due to the local ordering of P atoms in concentric circles. However, the packing of P atoms for the lipids contacting Aβ has less pronounced tendency to show such oscillation. We conclude that Aβ interaction causes a disturbance of local ordering of P atoms. We also computed the order parameter S_{cd} for the fatty acid tails for lipids and found that the difference between those forming contact with Aβ peptide and those in Aβ-free region was insignificant. In conclusion, we note that contact with Aβ causes

disturbance of lipid ordering in the monolayer, as signified by the local area per lipid and P atom radial pair correlation function.

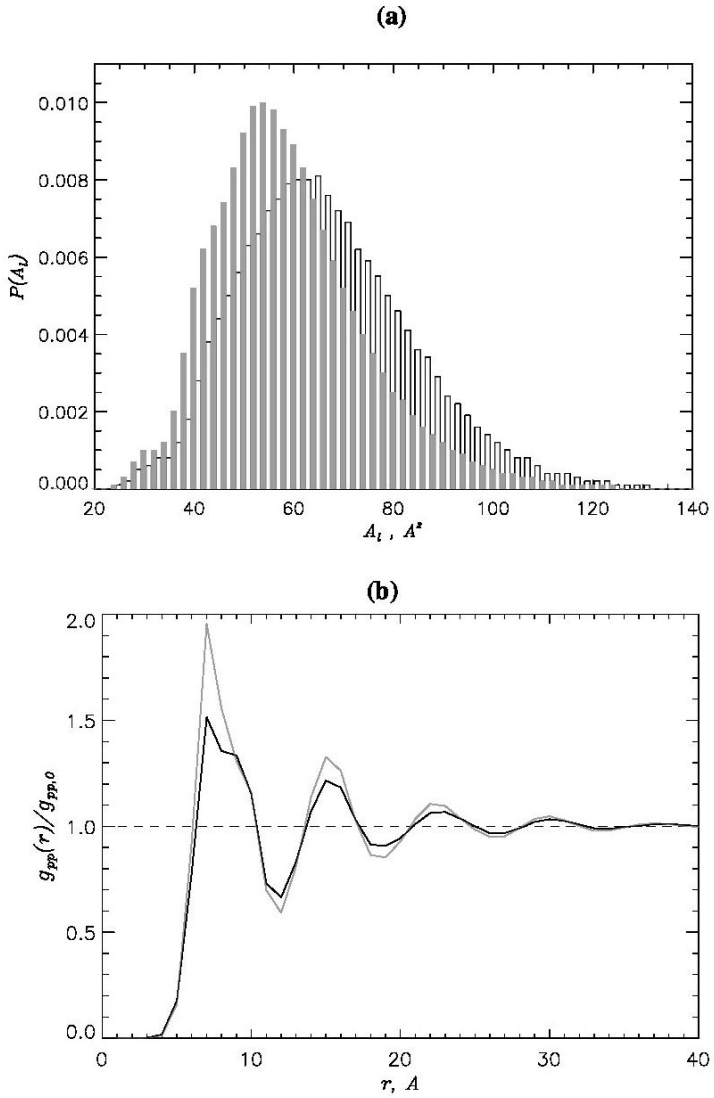

Figure 23 *(a) Distribution of local area per lipid for lipids contacting with the peptide (gray bar) or away from the peptide (open bar). (b) Averaged radial pair correlation function for P atoms* $g_{PP}(r)$ *for lipids near (black) or far from (gray) the bound peptide.*

6.2 Discussion

We studied the interaction of $A\beta_{10-40}$ monomer with DMPC monolayer using SASA implicit solvent model combined with CHARMM19 force field and replica exchange molecular dynamics (REMD). In order to validate the novel implicit solvent model for the monolayer, we demonstrated that our model shows good agreement with the experimental values of lipid order parameter S_{cd} (**Figure 3a**) and with explicit solvent simulation results for combined amino acid and bilayer system. We showed that at 360 K, the monomer binds to the monolayer with high affinity. Previous computational and experimental studies have indicated that $A\beta_{1-40}$ adsorbs unto the headgroup of zwitterionic membrane such as DPPC without insertion [67, 68, 69]. An implicit membrane model study of the insertion of Aβ monomer into lipid bilayer also showed that $A\beta_{1-40}$ peptide tends to reside at the membrane-water interface [70, 71]. Similar result was obtained using explicit water simulation [72].

We examined the atomic level interactions between Aβ monomer and DMPC monolayer and identified residues responsible for binding to be Tyr10, His13, Lys16, Phe20 and Lys28, which are either aromatic or positively charged. We also computed the probabilities of penetration of amino acids into the hydrophobic core region of the monolayer and found that the aromatic residues show higher probability to penetrate and interact with glycerol and fatty acid groups, while the charged residues tend to interact with the zwitterionic head groups of the lipid. This is in good qualitative agreement with the study of Tieleman and coworkers on the partitioning of amino acids in DOPC lipid

bilayer [55]. Buchete and coworkers studied the interaction of Aβ fibril protofilament with the bilayer and also observed that charged amino acids are the main binding factors [73].

We studied the impact of monolayer interaction on the Aβ monomer's structure, as compared to the monomer in water. We discovered that binding to the monolayer increases the peptide end-to-end distance, causes the loss in intrapeptide contacts and increases the strand content. To further illustrate the change in the secondary structure of Aβ peptide, we computed the averaged relative orientation $s(k)$ between two bond vectors against their distance along the primary sequence. Specifically, we computed the average cosine of the angles between the two bond vectors separated by k amino acids. The result is shown in **Figure 24a** for Aβ monomer in water, for Aβ peptide in dimer formation and for Aβ monomer interacting with monolayer. In water, $s(k)$ presents an oscillating pattern with approximate period of 4, a tendency also evident in Aβ dimer. These oscillations are the signatures of helix formation in those systems. On the other hand, $s(k)$ for Aβ monomer in contact with the monolayer shows only monotonic decrease, which is another indication that the helical content is lost due to the monolayer binding.

In order to further characterize the nature of this change in secondary structure, we plot in **Figure 24b** the dependence between the secondary structure content and the number of peptide-monolayer contacts. It is shown in the plot that the increase in peptide-monolayer contacts positively correlates with the increase in the β-strand content. We also observe

the negative correlation between the helix and strand content, confirming the helix to strand conversion induced by the monolayer interaction.

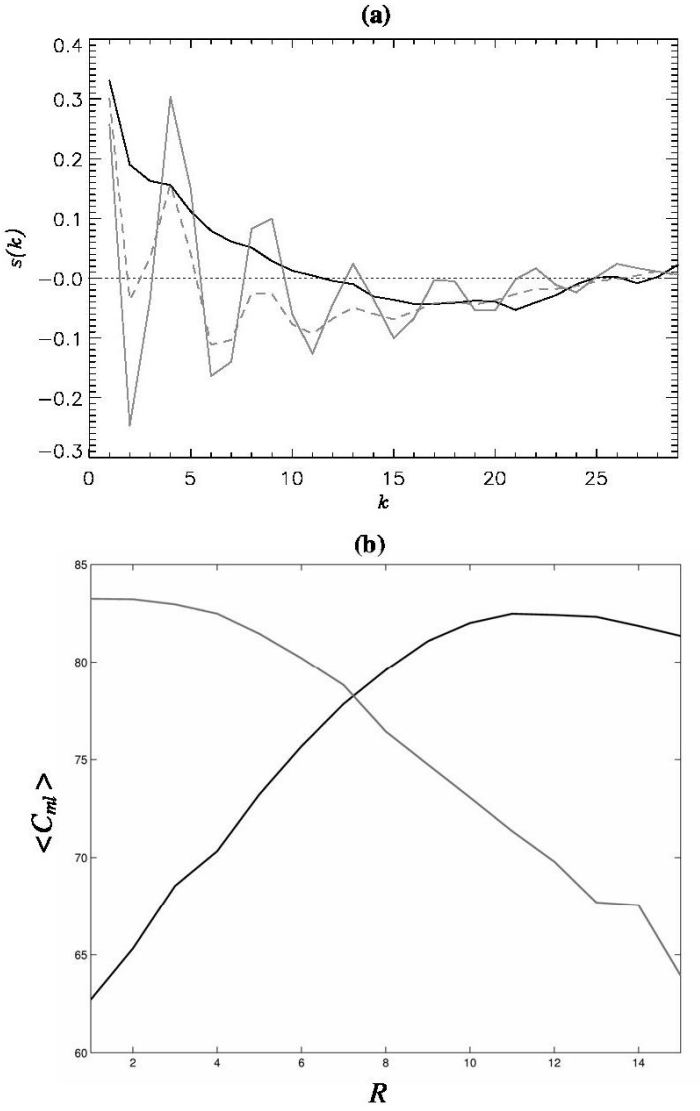

Figure 24 *(a) Autocorrelation function s(k) measuring the average orientation of two bond vectors separated by k amino acids. Data for monomer in water, dimer, and monomer bound to the monolayer are shown by gray, gray dashed and black lines. (b) Dependence between the number of residues R in helix (gray line) or strand (black line) conformation and the number of peptide-monolayer contacts* $<C_{ml}>$.

Recently, Jiang et al. studied Aβ monomer inserted in DPPC bilayer in the helical configuration for 90 ns [74]. They observed that the peptide tends to exit the bilayer and bind to the head group, while retaining the helical structure. The discrepancy with our study is likely due to the long time scales necessary for the Aβ monomer in helix conformation to unravel when bound to the lipid bilayer.

Another important observation is the effect of peptide binding on the monolayer. We showed that the area per lipid is diminished for the lipids in contact with Aβ monomer compared to those far from the peptide. We also observed that the ordering of P atoms in the lipid head groups is disturbed due to the interaction with peptide. These results are consistent with other studies observing that Aβ interaction perturbs the local lipid order [36, 65, 66].

6.3 Conclusion

Using novel force field for DMPC lipid consistent with the fast CHARMM19+SASA implicit solvent model, we built a system containing Aβ monomer and DMPC monolayer to study the structural characteristics of the peptide binding to the cellular membrane. Our statistically reliable results show that Aβ binding is largely driven by aromatic and charged amino acids. Aromatic residues are more prone to penetrate deeper into the hydrophobic core region of the monolayer, while charged residues tend to interact with the lipid head groups on the surface. We mapped the conformational ensemble of Aβ monomer bound to the lipid monolayer using clustering technique. We also showed that Aβ binding to the monolayer results in significant structural changes both in the peptide and lipids. This work is significant because it provides a statistically reliable description of the Aβ monomer-lipid monolayer interaction enabling more accurate assessment of the properties of the peptides bound to cellular membranes.

7. CONCLUSIONS AND FUTURE WORK

Using implicit solvent model and replica exchange molecular dynamics, we studied Aβ monomers and oligomers in aqueous environment or interacting with cofactors such as naproxen or DMPC monolayer. Investigating molecular details of Aβ oligomers interacting with cofactors is an essential step in understanding the pathology of and developing therapeutic agents against AD.

We elucidated the structural properties of Aβ oligomers and investigated the nature of monomer to oligomer transition. We used secondary structure analysis and conformational clustering to demonstrate that a profound structural change accompanies the oligomerization process,. We also characterized the antiaggregation effect of naproxen on Aβ dimers and compared it with the binding mechanism of naproxen for Aβ fibrils. The reasoning for the limited efficacy of naproxen as a therapeutic agent against AD was presented. Aβ monomer bound to the DMPC monolayer was studied, yielding an exhaustive sampling of conformational space. Residues responsible for monolayer binding were identified, and the nature of their interaction with the lipids was elucidated. It was found that the monolayer binding causes significant change in the structure of Aβ monomer, such as peptide extension, loss of intrapeptide interaction, and helix to strand conversion. The lipids in the monolayer also undergo structural disturbance upon peptide binding, which include closer packing and loss of order of the headgroups. Finally, a

novel force field was designed for the DMPC monolayer consistent with CHARMM19+SASA implicit solvent model.

It has to be pointed out that when one investigates a complex molecular system, a choice has to be made between computationally more expensive methodology and statistically more reliable data. The present research was focused on more efficient and fast model targeting simpler system, in order to achieve sufficient sampling of the conformational space. The results using implicit solvent model should be validated and complemented by explicit solvent model. The Aβ monomer-lipid monolayer system has a potential to be extended into many important directions. Useful insights can be gained using the lipid bilayer as a more realistic model for the cell membrane. An important example is examining the deeper penetration of Aβ peptide into lipid bilayer, for which the NPT ensemble must be used instead of the NVT ensemble chosen in the current study. Other types of lipids can be studied for this purpose, including the unsaturated and anionic lipids, which are known to be more prone for peptide insertion. Ultimately, the structural characterization of Aβ oligomers interacting with the core region of the lipid bilayers is of utmost importance in understanding the nature of peptide-membrane interaction. Several computational studies have been published, attempting to validate Aβ structures suggested upon experimental or computational grounds. Currently, however, it is very difficult to obtain statistically reliable sampling of conformational space. Devising the methodology to overcome these challenges will be a very exciting and active area of research in the future.

APPENDIX

For the implicit solvent model of DMPC lipids, the following modifications were made in topology top19_eef1.inp file:

```
RESI DMPC 0.00
GROUP               ! CHOLINE GROUP
ATOM N N -0.60
ATOM C13 CH3E 0.40
ATOM C14 CH3E 0.40
ATOM C15 CH3E 0.40
ATOM C12 CH2E 0.40
GROUP               ! PHOSPHORUS GROUP
ATOM C11 CH2E 0.10
ATOM P LP 1.50
ATOM O13 OT -0.78
ATOM O14 OT -0.78
ATOM O11 OM -0.57
ATOM O12 OS -0.57
ATOM C1 CH2E 0.10
GROUP               ! GLYCEROL GROUP
ATOM C2 CH1E 0.13
ATOM O21 OS -0.34
ATOM C21 C 0.63
ATOM O22 O -0.52
ATOM C22 CH2E 0.10
GROUP
ATOM C3 CH2E 0.13
ATOM O31 OS -0.34
ATOM C31 C 0.63
ATOM O32 O -0.52
ATOM C32 CH2E 0.10
GROUP               ! FATTY ACID GROUPS
ATOM C23 CH2E 0.00
ATOM C24 CH2E 0.00
```

```
ATOM C25 CH2E 0.00
ATOM C26 CH2E 0.00
ATOM C27 CH2E 0.00
ATOM C28 CH2E 0.00
ATOM C29 CH2E 0.00
ATOM C210 CH2E 0.00
ATOM C211 CH2E 0.00
ATOM C212 CH2E 0.00
ATOM C213 CH2E 0.00
ATOM C214 CH3E 0.00
GROUP
ATOM C33 CH2E 0.00
ATOM C34 CH2E 0.00
ATOM C35 CH2E 0.00
ATOM C36 CH2E 0.00
ATOM C37 CH2E 0.00
ATOM C38 CH2E 0.00
ATOM C39 CH2E 0.00
ATOM C310 CH2E 0.00
ATOM C311 CH2E 0.00
ATOM C312 CH2E 0.00
ATOM C313 CH2E 0.00
ATOM C314 CH3E 0.00
BOND N C13 N C14 N C15
BOND N C12
BOND C12 C11
BOND C11 O12
BOND O12 P P O11 P O13 P O14
BOND C1 C2 C1 O11
BOND C2 C3 C2 O21
BOND C3 O31
BOND O21 C21
BOND C21 C22
DOUBLE C21 O22
BOND C22 C23 C23 C24 C24 C25
BOND C25 C26 C26 C27 C27 C28
BOND C28 C29 C29 C210 C210 C211
BOND C211 C212 C212 C213 C213 C214
BOND O31 C31
```

```
BOND C31 C32
DOUBLE C31 O32
BOND C32 C33 C33 C34 C34 C35
BOND C35 C36 C36 C37 C37 C38
BOND C38 C39 C39 C310 C310 C311
BOND C311 C312 C312 C313 C313 C314
DIHE C13 N C12 C11 N C12 C11 O12 C12 C11 O12 P
DIHE C11 O12 P O11 O12 P O11 C1 P O11 C1 C2
DIHE C1 C2 C3 O31 C1 C2 O21 C21 C2 O21 C21 C22
DIHE O21 C21 C22 C23 C21 C22 C23 C24 C22 C23 C24 C25
DIHE C23 C24 C25 C26 C24 C25 C26 C27 C25 C26 C27 C28
DIHE C26 C27 C28 C29 C27 C28 C29 C210 C28 C29 C210 C211
DIHE C29 C210 C211 C212 C210 C211 C212 C213
DIHE C211 C212 C213 C214
DIHE O11 C1 C2 C3 C2 C3 O31 C31 C3 O31 C31 C32
DIHE C31 C32 C33 C34 C32 C33 C34 C35 C33 C34 C35 C36
DIHE C34 C35 C36 C37 C35 C36 C37 C38 C36 C37 C38 C39
DIHE C37 C38 C39 C310 C38 C39 C310 C311 C39 C310 C311 C312
DIHE C310 C311 C312 C313 C311 C312 C313 C314
DIHE C2 O21 C21 O22 C3 O31 C31 O32
DIHE O11 C1 C2 O21
IMPH C21 O21 C22 O22 C31 O31 C32 O32
IC C2 C1 O11 P 0.0 0.0 180.0 0.0 0.0
IC C1 O11 P O12 0.0 0.0 180.0 0.0 0.0
IC O11 O12 *P O13 0.0 0.0 120.0 0.0 0.0
IC O11 O12 *P O14 0.0 0.0 240.0 0.0 0.0
IC O11 P O12 C11 0.0 0.0 180.0 0.0 0.0
IC P O12 C11 C12 0.0 0.0 180.0 0.0 0.0
IC O12 C11 C12 N 0.0 0.0 180.0 0.0 0.0
IC C11 C12 N C13 0.0 0.0 180.0 0.0 0.0
IC C12 C13 *N C14 0.0 0.0 120.0 0.0 0.0
IC C12 C13 *N C15 0.0 0.0 240.0 0.0 0.0
IC O11 C1 C2 C3 0.0 0.0 120.0 0.0 0.0
IC C1 C2 C3 O31 0.0 0.0 180.0 0.0 0.0
IC C1 C3 *C2 O21 0.0 0.0 -120.0 0.0 0.0
IC C1 C2 O21 C21 0.0 0.0 180.0 0.0 0.0
IC C2 O21 C21 C22 0.0 0.0 120.0 0.0 0.0
IC O21 C21 C22 C23 0.0 0.0 180.0 0.0 0.0
IC C22 O21 *C21 O22 0.0 0.0 180.0 0.0 0.0
```

```
IC C21 C22 C23 C24 0.0 0.0 180.0 0.0 0.0
IC C22 C23 C24 C25 0.0 0.0 180.0 0.0 0.0
IC C23 C24 C25 C26 0.0 0.0 180.0 0.0 0.0
IC C24 C25 C26 C27 0.0 0.0 180.0 0.0 0.0
IC C25 C26 C27 C28 0.0 0.0 180.0 0.0 0.0
IC C26 C27 C28 C29 0.0 0.0 180.0 0.0 0.0
IC C27 C28 C29 C210 0.0 0.0 180.0 0.0 0.0
IC C28 C29 C210 C211 0.0 0.0 180.0 0.0 0.0
IC C29 C210 C211 C212 0.0 0.0 180.0 0.0 0.0
IC C210 C211 C212 C213 0.0 0.0 180.0 0.0 0.0
IC C211 C212 C213 C214 0.0 0.0 180.0 0.0 0.0
IC C2 C3 O31 C31 0.0 0.0 -120.0 0.0 0.0
IC C3 O31 C31 C32 0.0 0.0 180.0 0.0 0.0
IC O31 C31 C32 C33 0.0 0.0 180.0 0.0 0.0
IC C32 O31 *C31 O32 0.0 0.0 180.0 0.0 0.0
IC C31 C32 C33 C34 0.0 0.0 180.0 0.0 0.0
IC C32 C33 C34 C35 0.0 0.0 180.0 0.0 0.0
IC C33 C34 C35 C36 0.0 0.0 180.0 0.0 0.0
IC C34 C35 C36 C37 0.0 0.0 180.0 0.0 0.0
IC C35 C36 C37 C38 0.0 0.0 180.0 0.0 0.0
IC C36 C37 C38 C39 0.0 0.0 180.0 0.0 0.0
IC C37 C38 C39 C310 0.0 0.0 180.0 0.0 0.0
IC C38 C39 C310 C311 0.0 0.0 180.0 0.0 0.0
IC C39 C310 C311 C312 0.0 0.0 180.0 0.0 0.0
IC C310 C311 C312 C313 0.0 0.0 180.0 0.0 0.0
IC C311 C312 C313 C314 0.0 0.0 180.0 0.0 0.0
PATC FIRS NONE LAST NONE
```

The following parameters for bond length, bond angle, dihedral angle and Lennard-Jones potentials were added to parameter param19_eef1.inp file:

```
BONDS
CH1E OS 292.0 1.516
CH2E OS 320.0 1.696
OS LP 230.0 1.555
CH2E OM 320.0 1.696
OM LP 230.0 1.555
OT LP 525.0 1.546
```

```
CH3E N 422.0 1.45
ANGLES
CH3E N CH3E 60.0 109.5
CH2E CH2E OS 45.0 113.6
CH2E OS LP 50.0 115.3
CH2E OM LP 50.0 115.3
OS LP OT 85.0 103.9
OS LP OS 85.0 104.9
OS LP OM 85.0 104.9
OT LP OT 85.0 121.0
OT LP OM 85.0 121.0
CH1E CH2E OS 60.0 108.5
CH1E CH2E OM 60.0 108.5
CH2E CH1E OS 60.0 100.5
CH2E CH1E CH2E 50.0 117.1
CH1E OS C 50.0 115.5
CH2E OS C 50.0 115.5
DIHE
X CH1E OS X 0.7 1 180.0
X CH2E OS X 0.0 3 0.0
X CH2E OM X 0.0 3 0.0
X OS LP X 0.75 3 60.0
X OM LP X 0.75 3 60.0
CH2E CH1E CH2E OM 2.0 1 -120.0  ! to fix theta1
CH2E CH1E CH2E OS 2.0 1 0.0
CH1E OS C O 2.0 1 180.0         ! to fix beta2
CH2E OS C O 2.0 1 180.0         ! to fix gamma2
NONBONDED
OT 0 -0.120 1.70
LP 0 -0.585 2.15
```

REFERENCES

[1] Brookmeyer R, Johnson E, Ziegler-Graham K, MH Arrighi (2007). "Forecasting the global burden of Alzheimer's disease". Alzheimer's and Dementia. 3(3): 186–91.

[2] Hardy, J., & Selkoe, D. J. (2002) The amyloid hypothesis of Alzheimer's disease: progess and problems on the road to therapeutics. Science. 297, 353-356

[3] Lomakin, A., Chung, D. S., Benedek, G. B., Kirschner, D. A., Teplow, D. B. (1996) The role of APP processing and trafficking pathways in the formation of amyloid β-protein. Proc. Natl. Acad. Sci. USA. 93, 1125-1129

[4] Urbanc, B., Betnel, M., Cruz, L., Bitan, G., Teplow, D. B. (2010) Elucidation of amyloid β-protein oligomerization mechanisms: discrete molecular dynamics study. J. Am. Chem. Soc. 132, 4266-4280

[5] Sgourakis, N. G., Yan, Y. L., McCallum, S. A., Wang, C. Y., Garcia, A. E. (2007) The Alzheimer's peptides Aβ40 and 42 adopt distinct conformations in water: a combined MD/NMR study. J. Mol. Biol. 368, 1448-1457

[6] Hou, L., Shao, H., Zhang, Y., Li, H., Menon, N. K., Neuhaus, E. B., Brewer, J. M., Byeon, I.-J., Ray, D. G., Vitek, M. P., Iwashita, T., Makula, R. A., Przybyla, A. B., Zagorski, M. G. (2004) Solution NMR studies of the Aβ(1-40) and Aβ(1-42) peptides establish that the Met35 oxidation state affects the mechanism of amyloid formation. J. Am. Chem. Soc. 126, 1992-2005

[7] Urbanc, B., Cruz, L., Yun, S., Buldyrev, S. V., Bitan, G., Teplow, D. B., Stanley, H. E. (2004) In silico study of amyloid β-protein folding and oligomerization. Proc. Natl. Acad. Sci. USA. 101, 17345-17350

[8] Cote, S., Laghaei, R., Derreumaux, P., Mousseau, N. (2012) Distinct dimerization for various alloforms of the Amyloid-β protein: Aβ1-40, Aβ1-42, and Aβ1-40(D23N). J. Phys. Chem. B 116, 4043-4055

[9] Yang, M., Teplow, D. B. (2008) Amyloid β-protein monomer folding: free-energy surfaces reveal alloform-specific differences. J. Mol. Biol. 384, 450-464

[10] Dobson, C. M. (2003) Protein folding and misfolding. Nature. 426, 884-890

[11] Cheon, M., Chang, I., Mohanty, S., Luheshi, L. M., Dobson, C. M., Vendruscolo, M., Favrin, G. (2007) Structural reorganization and potential toxicity of oligomeric species formed during the assembly of amyloid fibrils. PLoS Comp. Biol. 3, 1727-1738

[12] Ahmed, M., Davis, J., Aucoin, D., Sato, T., Ahuja, S. Aimoto, S., Elliott, J. I., Nostrand, W. E., Smith, S. O. (2010) Structural conversion of neurotoxic amyloid-β1-42 oligomers to fibrils. Nat. Struct. Mol. Biol. 17, 561-568

[13] Kayed, R., Head, E., Thompson, J. L., McIntire, T. M., Milton, S. C., Cotman, C. W., Glabe, C. G. (2003) Common structure of soluble amyloid oligomers implies common mechanism of pathogenesis. Science. 300, 486-489

[14] Haass, C., Selkoe, D. J. (2007) Soluble protein oligomers in neurodegeneration: lessons from the Alzheimer's amyloid β-peptide, Nat. Rev. Mol. Cell Biol. 8, 101-112

[15] Gandy, S., Simon, A. J., Steele, J. W., Lublin, A. L., Lah, J. J., Walker, L. C., Levey, A. I., Krafft, G. A., Levy, E., Checler, F., Glabe, C., Bilker, W. B., Abel, T., Schmeidler, J., Ehrlich, M. E. (2010) Days to criterion as an indicator of toxicity associated with human Alzheimer amyloid-β oligomers. Ann. Neurol. 68, 220-230

[16] Chen, J., Armstrong, A. H., Koehler, A., Hecht, M. H. (2010) Small molecule microarrays enable the discovery of compounds that bind the Alzheimer's Aβ peptide and reduce its cytotoxicity. J. Am. Chem. Soc. 132, 17015-17022

[17] Shankar, G. M., Li, S., Mehta, T. H., Garcia-Munoz, A., Shepardson, N. E., Smith, I., Brett, F. M., Farrell, M. A., Rowan, M. J., Lemere, C. A., Regan, C. M., Walsh, D. M., Sabatini, B. L., Selkoe, D. J. (2008) Amyloid β-protein dimers isolated directly from Alzheimer's brains impair synaptic plasticity and memory. Nat. Med. 14, 837-842

[18] Ono, K., Condron, M. M., Teplow, D. B. (2009) Structure-neurotoxicity relationships of amyloid β-protein oligomers. Proc. Natl. Acad. Sci. USA. 106, 14745-14750

[19] Takeda, T., Klimov, D. K. (2009) Interpeptide interactions induce helix to strand structural transition in Aβ peptides. Proteins 77, 1-13

[20] Cole, G. M., Frautschy, S. A. (2010) Mechanisms of action of non-steroidal anti-inflammatory drugs for the prevention of Alzheimer's disease. CNS Neurol. Disord. Drug Targets. 9, 140-148

[21] Hirohata, M., Ono, K., Naiki, H., & Yamada, M. (2005). Non-steroidal anti-inflammatory drugs have anti-amyloidogenic effects for Alzheimer's β-amyloid fibrils in vitro. Neuropharmacology. 49, 1088-1099.

[22] Agdeppa, E. D., Kepe, V., Petric, A., Satyamurthy, N., Liu, J., Huang, S.-C., Small, G. W., Cole, G. M. & Barrio, J. R. (2003). In vitro detection of (s)-naproxen and ibuprofen binding to plaques in the Alzheimer's brain using the positron emission tomography molecular imaging probe 2-(1-{6-[(2-[18F]fluoroethyl)(methyl)amino]-2-naphthyl}ethylidene) malononitrile. Neurosci. 117, 723–730.

[23] Varvel, N. H., Bhaskar, K., Kounnas, M. Z., Wagner, S. L., Yang, Y., Lamb, B. T., Herrup, K. (2009) NSAIDs prevent, but do not reverse, neuronal cell cycle reentry in a mouse model of Alzheimer disease. J. Clin. Invest. 119, 3692-3702

[24] Raman, E. P., Takeda, T., Klimov, D. K. (2009) Molecular dynamics simulations of ibuprofen binding to Aβ peptides. Biophys. J. 97, 2070-2079

[25] Takeda, T., Chang, W. E., Raman, E. P., Klimov, D. K. (2010) Binding of non-steroidal anti-inflammatory drugs to Aβ fibril. Proteins 78, 2849-2860

[26] Takeda, T., Kumar, R., Raman, E. P., Klimov, D. K. (2010) Nonsteroidal anti-inflammatory drug naproxen destabilizes Aβ amyloid fibrils: a molecular dynamics investigation. J. Phys. Chem. B 114, 15394-15402

[27] Williams, T. L., Serpell, L. C. (2011) Membrane and surface interactions of Alzheimer's Aβ peptide – insights into the mechanism of cytotoxicity, FEBS J 278, 3905-3917

[28] Zhao, L. N., Long, H. W., Mu, Y., Chew, L. Y. (2012) The toxicity of Amyloid β oligomers. Int. J. Mol. Sci. 13, 7303-7327

[29] Meier, M., Seelig, J. (2007) Thermodynamics of the coil <=> β-sheet transition in a membrane environment. J. Mol. Biol. 369, 277-289

[30] Sun, Y., Lee, C.-C., Chen, T.-H., Huang, H. W. (2010) Kinetic process of β-amyloid formation via membrane binding. Biophys. J. 99, 544-552

[31] Wahlstroem, A., Hugonin, L., Peralvarez-Marin, A., Jarvet, J., Graslund, A. (2008) Secondary structure conversions of Alzheimer's Aβ(1-40) peptide induced by membrane-mimicking detergents. FEBS Journal 275, 5117-5128

[32] Nikolic, A., Baud, S., Rauscher, S., Pomes, R. (2011) Molecular mechanism of β-sheet self-organization at water-hydrophobic interface. Proteins, Struct. Func. Bioinf. 79, 1-22

[33] Jean, L., Lee, C. F., Vaux, D. J. (2012) Enrichment of amyloidogenesis at an air-water interface. Biophys. J. 102:1154-1162

[34] Morriss-Andrews, A., Bellesia, G., Shea, J.-E. (2012) β-sheet propensity controls the kinetic pathways and morphologies of seeded peptide aggregation. J Chem Phys 137:145104

[35] Kremer, J. J., Sklansky, D. J., Murphy, R. M. (2001) Profile of changes in lipid bilayer structure caused by β-amyloid peptide. Biochemistry, 40, 8563–8571

[36] Poojari, C., Kukol, A., Strodel, B. (2013) How the amyloid-β peptide and membranes affect each other: An extensive simulation study. Biochim. Biophys. Acta 1828, 327-339

[37] Valincius, G., Heinrich, F., Budvytyte, R., Vanderah, D. J., McGillivray, D. J., Sokolov, Y., Hall, J. E., Loesche, M. (2008) Soluble amyloid β-oligomers affect dielectric membrane properties by bilayer insertion and domain formation: implications for cell toxicity. Biophys. J. 95, 4845-4861

[38] Wong, P. T., Schauerte, J. A., Wisser, K. C., Ding, H., Lee, E. L., Steel, D. G., Gafni, A. (2009) Amyloid-β membrane building and permeabilization are distinct processes influenced separately by membrane charge and fluidity. J. Mol. Biol. 386, 81-96

[39] Arispe, N., Diaz, J. C. & Simakova, O. (2007) Aβ ion channels. Prospects for treating Alzheimer'sdisease with Aβ channel blockers. Biochim. Biophys. Acta 1768, 1952–1965.

[40] Kawahara, M., Ohtsuka, I., Yokoyama, S., Kato-Negishi, M., Sadakane, Y. (2011) Membrane incorporation, channel formation, and disruption of Calcium homeostasis by Alzheimer's β-amyloid protein, Int. J. Alz. Dis. 2011, 304583

[41] Qulst, A., Doudevski, I., Lin, H., Azimova, R., Ng, D., Franglone, B., Kagan, B., Ghiso, J., Lal, R. (2005) Amyloid ion channels: a common structural link for protein-misfolding disease. Proc. Natl. Acad. Sci. USA. 102, 10427-10432

[42] Vitalis, A., Caflisch, A. (2010) Micelle-like architecture of the monomer ensemble of Alzheimer's amyloid-β peptide in aqueous solution and its implications for Aβ aggregation. J. Mol. Biol. 403, 148-165

[43] Ferrara, P., Apostokalis, J., Caflisch, A. (2002) Evaluation of a fast implicit solvent model for molecular dynamics simulation. Proteins 46, 24-33

[44] Kim, S., Takeda, T., Klimov, D. K. (2010) Globular state in the oligomers formed by Aβ peptides. J. Chem. Phys. 132, 225101

[45] Kim, S., Takeda, T., Klimov, D. K. (2010) Mapping conformational ensembles of Aβ oligomers in molecular dynamics simulations. Biophys. J. 99, 1949-1958

[46] Kim, S., Chang, W. E., Kumar, E., Klimov, D. K. (2011) Naproxen interferes with the assembly of Aβ oligomers implicated in Alzheimer's disease. Biophys. J. 100, 2024-2032

[47] Kim, S., Klimov, D. K. (2013) Binding to the lipid monolayer induces conformational transition in Aβ monomer. J. Mol. Model. 19, 737-750

[48] Takeda, T., Klimov, D. K. (2009) Probing the effect of amino-terminal truncation for Aβ1-40 peptides. J. Phys. Chem. B 113, 6692-6702

[49] Brooks, B. R., Bruccoler, R. E., Olafson, B. D., States, D. J., Swaminathan, S., Karplus, M. (1983) CHARMM: a program for macromolecular energy, minimization, and dynamics. J. Comput. Chem. 4, 187-217

[50] Straub, J. E., Thirumalai, D. (2011) Toward a molecular theory of early and late events in monomer to amyloid fibril formation. Annu. Rev. Phys. Chem. 62, 437-463

[51] Kasson, P. M., Pande, V. S. (2004) Molecular dynamics simulation of lipid reorientation at bilayer edges. Biophys. J. 86, 3744-3749

[52] Karplus, M., et al. (1995) An all-atom empirical energy function for the simulation of nucleic acids. J. Am. Chem. Soc. 117, 11946-11975

[53] Lazaridis, T., Mallik, P., Chen, Y. (2005) Implicit Solvent Simulations of DMPC Micelle Formation. J. Phys. Chem. B 109, 15098-15106

[54] Aussenac, F., Laguerre, M., Schmitter, J.-M., Dufourc, E., J. (2003) Detailed structure and dynamics of bicelle phospholipids using selectively deuterated and perdeuterated labels. 2H NMR and molecular mechanics study. Langmuir, 19:10468–10479

[55] MacCallum, J. L., Bennett, W. F. D., Tieleman, D. P. (2008) Distribution of amino acids in a lipid bilayer from computer simulations. Biophys. J., 94, 3393–3404

[56] Sugita, Y., Okamoto, Y. (1999) Replica-exchange molecular dynamics method for protein folding. Chem. Phys. Lett. 114, 141-151

[57] Kabsch, W., Sander, C. (1983) Dictionary of protein secondary structure: pattern recognition of hydrogen-bonded and geometrical features. Biopolymers. 22, 2577-2637

[58] Klimov, D. K., Thirumalai, D. (1998) Lattice models for proteins reveal multiple folding nuclei for nucleation-collapse mechanism. J. Mol. Biol. 282, 471-492

[59] Ferrenberg, A. M., Swendsen, R. H. (1989) Optimized Monte Carlo data analysis. Phys. Rev. Lett. 63, 1195-1198

[60] Takeda, T., Klimov, D. K. (2009) Replica exchange simulations of the thermodynamics of Aβ fibril growth. Biophys. J. 96, 442-452

[61] Essex, J., W., Hann, M. M., Richards, W. G. (1994) Molecular dynamics simulations of a hydrated phospholipid bilayer. Philos. Trans. Biol. Sci., 344:239–260

[62] Landau, L. D., Lifshitz, E. M. (1984) Course on Theoretical Physics, Statistical Physics (Butterworth-Heinemann, Oxford), Vol. 5

[63] Grosberg, A. Y., Khokhlov, A. R. (1994) Statistical Physics of Macromolecules (AIP, Woodbury)

[64] Yang, F., Lim, G. P., Begum, A. N., Ubeda, O. J., Simmons, M. R., Ambegaokar, S. S., Chen, P. P., Kayed, R., Glabe, C. G., Frautschy, S. A., Cole, G. M. (2005) Curcumin inhibits formation of amyloid β oligomers and fibrils, binds plaques, and reduces amyloid in vivo. J. Biol. Chem. 280, 5892-5901

[65] Lemkul, J. A., Bevan, D. R. (2008) A comparative molecular dynamics analysis of the amyloid β-peptide in a lipid bilayer. Archiv. Biochem. Biophys. 470, 54-63

[66] Lemkul, J. A., Bevan, D. R. (2009) Perturbation of membranes by the amyloid β-peptide – a molecular dynamics study. FEBS J. 276, 3060-3075

[67] Davis, C. H., Berkowitz, M. L. (2009) Structure of the amyloid-β (1-42) monomer absorbed to model phospholipid bilayers: a molecular dynamics study. J. Phys. Chem. B 113, 14480-14486

[68] Davis, C. H., Berkowitz, M. L. (2009) Interaction between Amyloid-β (1-42) peptide and phospholipid bilayers: A molecular dynamics study. Biophys. J. 96, 785-797

[69] Davis, C. H., Berkowitz, M. L. (2010) A molecular dynamics study of the early stages of amyloid-β (1-42) oligomerization: The role of lipid membranes. Proteins, Struct. Func. Bioinf. 78, 2533-2545

[70] Ege, C., Lee, K. Y. C. (2004) Insertion of Alzheimer's Aβ40 peptide into lipid monolayers. Biophys. J. 87, 1732-1740

[71] Miyashita, N., Straub, J. E., Thirumalai, D. (2009) Structures of β-amyloid peptide 1-40, 1-42, and 1-55 – the 672-726 fragment of APP – in a membrane environment with implications for interactions with gamma-secretase. J. Am. Chem. Soc. 131, 17843-17852

[72] Qiu, L., Buie, C., Reay, A., Vaughn, M. W., Cheng, K. H. (2011) Molecular dynamics simulations reveal the protective role of cholesterol in β-amyloid protein-induced membrane disruptions in neuronal membrane mimics. J. Phys. Chem. B 115, 9795-9812

[73] Tofoleanu, F., Buchete, M. V. (2012) Molecular interactions of Alzheimer's Aβ protofilaments with lipid membranes. J. Mol. Biol. 421, 572-586

[74] Xu, Y., Shen, J., Luo, X., Zhu, W., Chen, K., Ma, J., Jiang, H. (2005) Conformational transition of amyloid β-peptide. Proc. Natl. Acad. Sci. USA 102, 5403-5407

CURRICULUM VITAE

Seongwon Kim received his Bachelor of Science from Korea Advanced Institute of Science and Technology, Taejon, Korea, in 1990. He received his Doctor of Philosophy in Mathematics from New York University, New York, New York, in 1998 and his Master of Divinity from Presbyterian College and Theological Seminary, Seoul, Korea, in 2004. He has been ministering as an Educator for the Presbyterian Church (USA) for eight years.